The Astrophysical Journal, 730:23 (16pp), 2011 March 20 doi:10.1088/0004-637X/730/1/23

THE *HST*/ACS COMA CLUSTER SURVEY. IV. INTERGALACTIC GLOBULAR CLUSTERS AND THE MASSIVE GLOBULAR CLUSTER SYSTEM AT THE CORE OF THE COMA GALAXY CLUSTER*

Eric W. Peng[1,2,3], Henry C. Ferguson[3], Paul Goudfrooij[3], Derek Hammer[4], John R. Lucey[5], Ronald O. Marzke[6], Thomas H. Puzia[7,8], David Carter[9], Marc Balcells[10], Terry Bridges[11], Kristin Chiboucas[12], Carlos del Burgo[13], Alister W. Graham[14], Rafael Guzmán[15], Michael J. Hudson[16], Ana Matković[17], David Merritt[18], Bryan W. Miller[19], Mustapha Mouhcine[9], Steven Phillipps[20], Ray Sharples[5], Russell J. Smith[5], Brent Tully[11], and Gijs Verdoes Kleijn[21]

[1] Department of Astronomy, Peking University, Beijing 100871, China; peng@pku.edu.cn
[2] Kavli Institute for Astronomy and Astrophysics, Peking University, Beijing 100871, China
[3] Space Telescope Science Institute, 3700 San Martin Drive, Baltimore, MD 21228, USA
[4] Department of Physics and Astronomy, Johns Hopkins University 3400 N. Charles St., Baltimore, MD 21228, USA
[5] Department of Physics, University of Durham, South Road, Durham DH1 3LE, UK
[6] Department of Physics & Astronomy, San Francisco State University, 1600 Holloway Avenue, San Francisco, CA 94132, USA
[7] National Research Council of Canada, Herzberg Institute of Astrophysics, 5071 West Saanich Road, Victoria, BC V9E 2E7, Canada
[8] Departmento de Astronomía y Astrofísica, Pontificia Universidad Católica de Chile, Av. Vicuña Mackenna 4860, 7820436 Macul, Santiago, Chile
[9] Astrophysics Research Institute, Liverpool John Moores University, Twelve Quays House, Egerton Wharf, Birkenhead CH41 1LD, UK
[10] Instituto de Astrofisica de Canarias, 38200 La Laguna, Tenerife, Spain
[11] Department of Physics, Engineering Physics and Astronomy, Queen's University, Kingston, ON K7L 3N6, Canada
[12] Institute for Astronomy, University of Hawai'i, 2680 Woodlawn Drive, Honolulu, HI 96822, USA
[13] School of Cosmic Physics, Dublin Institute for Advanced Studies, 31 Fitzwilliam Place, Dublin 2, Ireland
[14] Centre for Astrophysics and Supercomputing, Swinburne University of Technology, Hawthorn, Victoria 3122, Australia
[15] Department of Astronomy, University of Florida, P.O. Box 112055, Gainesville, FL 32611, USA
[16] Physics and Astronomy, University of Waterloo, 200 University Avenue West, Waterloo, Ontario, Canada N2L 3G1, Canada
[17] Department of Astronomy and Astrophysics, Pennsylvania State University, University Park, PA 16802, USA
[18] Center for Computational Relativity and Gravitation and Department of Physics, Rochester Institute of Technology, Rochester, NY 14623, USA
[19] Gemini Observatory, Casilla 603, La Serena, Chile
[20] Astrophysics Group, H. H. Wills Physics Laboratory, University of Bristol, Tyndall Avenue, Bristol BS8 1TL, UK
[21] Kapteyn Astronomical Institute, University of Groningen, P.O. Box 800, 9700 AV Groningen, The Netherlands
Received 2009 July 29; accepted 2010 December 20; published 2011 February 28

ABSTRACT

Intracluster stellar populations are a natural result of tidal interactions in galaxy clusters. Measuring these populations is difficult, but important for understanding the assembly of the most massive galaxies. The Coma cluster of galaxies is one of the nearest truly massive galaxy clusters and is host to a correspondingly large system of globular clusters (GCs). We use imaging from the *HST*/ACS Coma Cluster Survey to present the first definitive detection of a large population of intracluster GCs (IGCs) that fills the Coma cluster core and is not associated with individual galaxies. The GC surface density profile around the central massive elliptical galaxy, NGC 4874, is dominated at large radii by a population of IGCs that extend to the limit of our data ($R < 520$ kpc). We estimate that there are $47{,}000 \pm 1600$ (random) $^{+4000}_{-5000}$ (systematic) IGCs out to this radius, and that they make up ∼70% of the central GC system, making this the largest GC system in the nearby universe. Even including the GC systems of other cluster galaxies, the IGCs still make up ∼30%–45% of the GCs in the cluster core. Observational limits from previous studies of the intracluster light (ICL) suggest that the IGC population has a high specific frequency. If the IGC population has a specific frequency similar to high-S_N dwarf galaxies, then the ICL has a mean surface brightness of $\mu_V \approx 27$ mag arcsec^{-2} and a total stellar mass of roughly 10^{12} $\mathcal{M}_\odot$ within the cluster core. The ICL makes up approximately half of the stellar luminosity and one-third of the stellar mass of the central (NGC 4874+ICL) system. The color distribution of the IGC population is bimodal, with blue, metal-poor GCs outnumbering red, metal-rich GCs by a ratio of 4:1. The inner GCs associated with NGC 4874 also have a bimodal distribution in color, but with a redder metal-poor population. The fraction of red IGCs (20%), and the red color of those GCs, implies that IGCs can originate from the halos of relatively massive, L^* galaxies, and not solely from the disruption of dwarf galaxies.

Key words: galaxies: clusters: individual (Coma) – galaxies: elliptical and lenticular, cD – galaxies: evolution – galaxies: halos – galaxies: star clusters: general – globular clusters: general

Online-only material: color figures

1. INTRODUCTION

1.1. Intracluster Stellar Populations and Hierarchical Galaxy Formation

Massive elliptical galaxies at the centers of galaxy clusters—often brightest cluster galaxies (BCGs) and sometimes cD galaxies—generally have little ongoing star formation with only minor evolution since $z \sim 1$, and only a shallow relationship between their stellar mass and their host cluster mass (e.g., Lin & Mohr 2004; Whiley et al. 2008). In the standard hierarchical paradigm, however, the most massive halos should be the last to assemble, and so these galaxies have traditionally presented problems for formation models.

Recent simulations suggest that this paradox can be resolved in a picture where the stars that end up in the most massive galaxies form early, energy feedback from supernovae and active

* Based on observations with the NASA/ESA *Hubble Space Telescope* obtained at the Space Telescope Science Institute, which is operated by the Association of Universities for Research in Astronomy, Inc., under NASA contract NAS 5-26555.

galactic nuclei subsequently suppress star formation, and the assembly of these galaxies through dry mergers continues right up to the present day (De Lucia & Blaizot 2007; although see Bildfell et al. 2008 for evidence that feedback is not 100% efficient). Thus, even if there is little star formation at late times, these galaxies are still expected to further assemble stellar mass at $z < 2$. This predicted increase in the masses of BCGs over time, however, may be in conflict with observations that show little mass evolution of BCGs from $z \sim 1.5$ to the present (Collins et al. 2009).

It is expected that the dry merging or tidal stripping of satellites should not only contribute stars to the central galaxy itself, but also to an intracluster component that has previously been associated with the extended stellar envelopes of cD galaxies (Matthews et al. 1964), and is sometimes labeled as a "diffuse stellar component" (Monaco et al. 2006) or simply "intracluster light" (ICL). This component can make up a large fraction of the total luminosity at the center of galaxy clusters (Oemler 1976) and if added to the stellar mass of central cluster galaxies might naturally explain current contradictions between simulation and observation. Purcell et al. (2007) simulated the formation of the ICL from the shredding of satellite galaxies, finding that in massive clusters, the ICL can dominate the total stellar mass of the combined ICL+BCG system, which is consistent with observations of low redshift clusters (Gonzalez et al. 2005; Seigar et al. 2007).

In fact, there is increasing observational evidence that a significant fraction (10%–40%) of the total stellar light in a galaxy cluster is intergalactic. Starting with Zwicky (1951), many detections of low surface brightness starlight in galaxy clusters—both in cD envelopes and in the regions between galaxies—support the existence of substantial intracluster stellar populations (Welch & Sastry 1972; Uson et al. 1991; Vilchez-Gomez et al. 1994; Gregg & West 1998; Trentham & Mobasher 1998; Feldmeier et al. 2002, 2004a; Lin & Mohr 2004; Adami et al. 2005; Zibetti et al. 2005; Mihos et al. 2005; Gonzalez et al. 2005; Seigar et al. 2007; Gonzalez et al. 2007; Krick & Bernstein 2007). In nearby clusters, there have also been direct detections of intergalactic red giant branch stars (Ferguson et al. 1998), asymptotic giant branch stars (Durrell et al. 2002), planetary nebulae (Theuns & Warren 1997; Mendez et al. 1997; Feldmeier et al. 1998; Feldmeier et al. 2004b; Okamura et al. 2002; Arnaboldi et al. 2004; Gerhard et al. 2007; Arnaboldi et al. 2007; Castro-Rodriguéz et al. 2009; Doherty et al. 2009), novae (Neill et al. 2005), and supernovae (Gal-Yam et al. 2003). Detections of intergalactic light have also been made in compact groups (Da Rocha & Mendes de Oliveira 2005). These studies tend to show that the richer and more massive the group or cluster, the larger the fraction of intergalactic light.

1.2. Intergalactic Globular Clusters

Another important clue to the formation of massive ellipticals is that those residing at the centers of galaxy clusters often host extremely large populations of globular clusters (GCs). The star-forming events that form globular clusters will mostly form stars that end up in the field, so it is natural that the number of GCs in a galaxy should roughly scale with that galaxy's stellar luminosity or mass. However, the ratio of GCs to starlight—usually characterized as the specific frequency, S_N (Harris & van den Bergh 1981)—has long been known to vary across galaxy mass and morphology, with giant central elliptical galaxies harboring the largest GC systems and having some of the highest specific frequencies. This abundance of GCs in galaxy clusters appears explainable if the number of GCs scales with either total baryonic mass at the cluster center, including hot gas (McLaughlin 1999), or the total dynamical mass of the cluster (Blakeslee et al. 1997). Blakeslee (1997, 1999) observed that the number of GCs in galaxy clusters was directly related to cluster mass, but the relatively constant BCG luminosity thus led to high S_N. It is possible that the high specific frequencies are because measurements of the galaxy luminosity typically do not include a substantial ICL component, and that the high S_N in central cluster galaxies would be more normal if the ICL was included. Galaxy-specific frequency also varies with galaxy stellar mass (or luminosity) in a way that is consistent with the expected variation in galaxy stellar mass fraction (or mass-to-light ratio; Peng et al. 2008; Spitler & Forbes 2009).

This connection between GCs and total mass has interesting implications, particularly in massive galaxy clusters where the predicted build up of stellar mass in central galaxies should be paralleled by the build up of a large GC system. If much of the stellar mass in galaxy clusters resides in the low surface brightness ICL then there should also be a corresponding population of intracluster GCs (IGCs) that are not gravitationally bound to individual galaxies, but directly to the cluster itself. Moreover, the detection of point-source IGCs in the nearest clusters is a much easier observational endeavor than measuring the faint ICL, giving us a window onto the nature of the diffuse stellar content.

There are other reasons to expect substantial populations of IGCs. West (1993) proposed that GC formation may be biased toward the largest mass overdensities, i.e., galaxy clusters. West et al. (1995) also proposed that populations of IGCs were responsible for the high S_N seen in cD galaxies. More recently, spectroscopy of ultra-compact dwarfs (UCDs) and massive GCs (also dubbed dwarf-globular transition objects; Haşegan et al. 2005) have uncovered a population of compact stellar systems in galaxy clusters resembling the most massive GCs or dE nuclei stripped of their host galaxies (Drinkwater et al. 2003; Hilker et al. 2007; Mieske et al. 2008; Gregg et al. 2009; Madrid et al. 2010; Chiboucas et al. 2010). These objects, while generally more massive than typical GCs and consequently may have different origins, might be the so-called tip of the iceberg for a large population of free-floating, normal globular clusters.

In fact, a number of extragalactic GC studies over the past few years have strongly suggested the presence of IGCs in nearby galaxy clusters. In the Virgo and Fornax Clusters, serendipitous discoveries of GCs in intergalactic regions using *Hubble Space Telescope* (*HST*) imaging (Williams et al. 2007), ground-based imaging (Bassino et al. 2003), and spectroscopy (Bergond et al. 2007) point to the existence of IGC populations. However, it is often unclear whether these GCs are truly intergalactic or are part of the extended halos of cluster galaxies (c.f. Schuberth et al. 2008). A recent study by Lee et al. (2010), however, used data from the Sloan Digital Sky Survey (SDSS) and found statistically significant detections of GC candidates throughout the Virgo cluster. In more distant galaxy clusters, candidate IGC populations have been identified as point-source excesses in *HST* imaging (Jordán et al. 2003; West et al. 2011).

It is possible that some IGCs and intracluster stars formed in situ, i.e., in cold, intergalactic gas that never accreted onto or was stripped from galaxies. It is also possible that IGCs formed very early and at high efficiencies in dwarf-sized subhalos (e.g., Moore et al. 2006; Peng et al. 2008) and whose host galaxies were subsequently tidally destroyed by interactions with the cluster potential. Another possibility is that IGCs were formed in

larger galaxies and were stripped through tidal interactions with the cluster potential or with other galaxies (see, e.g., simulations of Yahagi & Bekki 2005; Bekki & Yahagi 2006).

The formation of the IGC population is obviously linked to that of the ICL, although the observed properties of the two populations may be different. For example, the detectability of the ICL is highly dependent on its surface brightness, whereas IGCs are detectable even in isolation. Simulations by Rudick et al. (2009) show that the ICL is supplied by tidal streams that originally have relatively high surface brightness but then disperse to become fainter and harder to detect. ICL studies using surface photometry are thus more sensitive to recent disruptions, whereas the IGC population is a less temporally biased tracer of the full intracluster stellar population.

The study of extragalactic GC systems has been transformed by the high spatial resolution imaging of the *HST*, with observations of hundreds of GC systems now in the archives and published literature (e.g., Jordán et al. 2009). *HST*'s deep sensitivity to compact or unresolved sources, and its ability to distinguish background galaxies from likely GCs, makes it an ideal tool for extragalactic GC studies. However, the relatively narrow field of view of *HST*'s cameras and the close proximity of the galaxies being studied ($D \lesssim 100$ Mpc) mean that most *HST* studies have focused on GC systems directly associated with galaxies. Observations of wider fields are usually conducted with ground-based telescopes (e.g., McLaughlin 1999; Bassino et al. 2006; Rhode et al. 2007) that gain area at the cost of spatial resolution.

1.3. The Coma Cluster of Galaxies

The Coma cluster of galaxies (Abell 1656) is one of the nearest rich, dense clusters, and is a fundamental target for extragalactic studies. Studies of GC systems in Coma from the ground using surface brightness fluctuations (Blakeslee et al. 1997; Blakeslee 1999) and using *HST* (Kavelaars et al. 2000; Harris et al. 2000, 2009) all point to large GC systems around the cluster's giant elliptical galaxies, particularly around the central massive galaxy, NGC 4874 (Harris et al. 2009). Although many photometric studies support the existence of an intracluster stellar light component in Coma (e.g., Zwicky 1951; de Vaucouleurs & de Vaucouleurs 1970; Welch & Sastry 1972; Kormendy & Bahcall 1974; Mattila 1977; Melnick et al. 1977; Thuan & Kormendy 1977; Bernstein et al. 1995; Gregg & West 1998; Calcáneo-Roldán et al. 2000; Adami et al. 2005) and even velocities for intracluster planetary nebulae have been measured (Gerhard et al. 2007; Arnaboldi et al. 2007), evidence for or against the existence of IGCs is much more muddled. A search for IGCs in Coma using ground-based data by Marín-Franch & Aparicio (2002, 2003) did not find a surface brightness fluctuation signal that would have hinted at the presence of IGCs, mainly because of the shallow limiting magnitude of their photometry.

At a distance of 100 Mpc, the value we adopt for this paper ($m - M = 35$; Carter et al. 2008), $1'$ on the sky subtends 29 kpc in the cluster, and the mean of the GC luminosity function (GCLF) in giant ellipticals is $I_{\rm Vega} = 26.44$ mag. This regime of projected areal coverage and GC apparent brightness makes it reasonable to conduct a contiguous survey of the Coma cluster core for GCs, unbiased by the locations of individual galaxies, using the *HST* Advanced Camera for Surveys (ACS) Wide Field Channel (WFC).

The *HST*/ACS Coma Cluster Survey is a Treasury Survey originally approved for 164 orbits. One of the main components of this survey was a contiguous ACS/WFC mosaic of the core of the Coma cluster, making it the ideal data set to investigate the existence of intergalactic GCs. Hints of this population have already appeared in studies of UCDs by Madrid et al. (2010) and Chiboucas et al. (2010). This paper presents the first compilation and description of IGCs in the Coma cluster.

2. OBSERVATIONS AND DATA

2.1. Imaging Data

The data used in this study are from the *HST*/ACS Coma Cluster Survey. The survey observations and data reduction are described in detail by Carter et al. (2008), the catalog generation for the public data release is described by Hammer et al. (2010), and an in-depth analysis of galaxy structural parameters and completeness is presented in Balcells et al. (2011). We summarize the relevant information here.

The Coma Cluster Survey, as originally designed, consisted of a large central ACS mosaic of the Coma cluster core, and 40 targeted observations in the outer regions of the cluster. The central mosaic was designed to be 42 contiguous ACS/WFC pointings in a 7×6 tiling configuration, and covering a $21' \times 18'$ area. Each pointing is observed in two filters, F475W (g) and F814W (I), with exposure times of 2560s and 1400s, respectively. Unfortunately, the failure of the ACS/WFC (2007 January) meant that only 28% of the survey was completed: 19 pointings in or around the central mosaic, and 6 in the outer regions. Within the core, the central galaxy NGC 4874 was observed, but the other giant elliptical, NGC 4889, was not imaged before the ACS failure. Despite the shortfall, the current observations still provide the largest set of deep, high-resolution imaging available for this important galaxy cluster. Recent studies of compact galaxies in Coma (Price et al. 2009) and spectroscopy of Coma cluster members (Smith et al. 2008) are part of a concerted effort to study galaxy evolution in the Coma cluster built around this *HST* Treasury survey.

The ACS data reduction was performed using a dedicated Pyraf/STSDAS pipeline that registered and combined images while performing cosmic-ray rejection. The dithered images were combined using Multidrizzle (Koekemoer et al. 2002), which uses the Drizzle algorithm (Fruchter & Hook 2002). For this study, we used the data drizzled for the ACS Coma Survey Data Release 2 (DR2). However, except for Visits 3, 10, and 57, the F814W images on which the bulk of this paper is based are identical to those in Data Release 1 (DR1).

2.2. Object Catalogs and Galaxy Subtraction

Our images of the Coma cluster reveal a striking amount of detail: cluster members across the mass spectrum, globular clusters, background galaxies, and a few foreground stars. Given the different spatial scales of these objects on the sky, it is important to generate catalogs with detection parameters optimized for the subject under study. For our purpose of studying the globular clusters *between* galaxies, we used the well-tested Source Extractor software package (Bertin & Arnouts 1996) with parameters optimized for point-source detection, and which are effectively identical to those used by Hammer et al. (2010) in the public data release.[22] Photometry was put on the AB magnitude system using the zero points of Sirianni et al. (2005). All magnitudes in this paper are AB unless otherwise specified.

[22] For details, visit the Coma Cluster Survey Web site at http://astronomy.swin.edu.au/coma/.

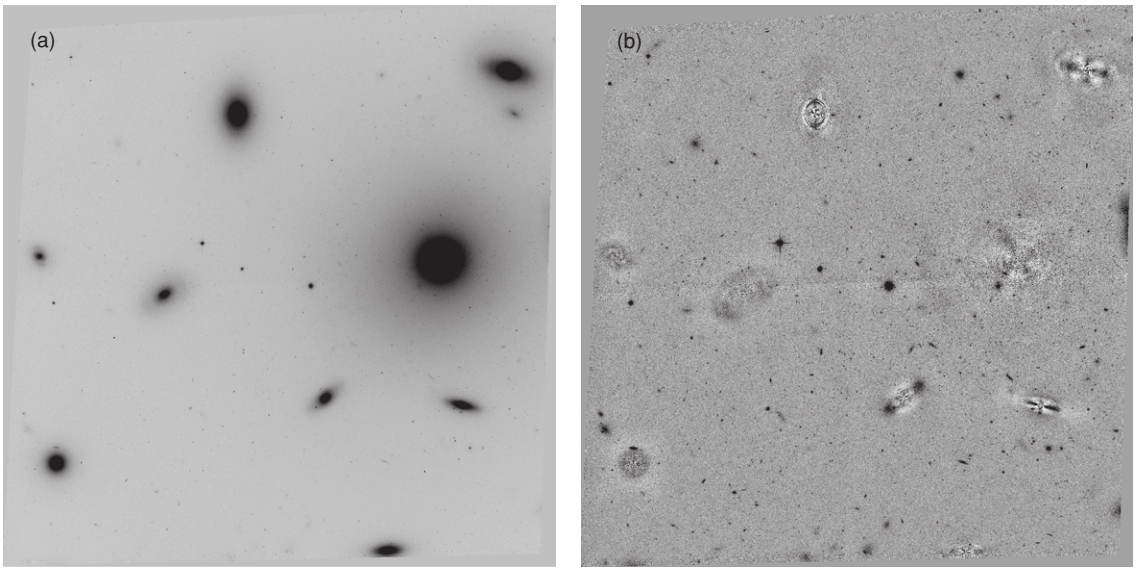

Figure 1. (a) ACS F814W image of the central pointing (Visit 19) containing NGC 4874 and many other bright elliptical galaxies. North is left and east is down. The image is 202″ (98 kpc) on a side. (b) The same pointing but after our iterative galaxy subtraction. Residuals at galaxy centers are still visible at this contrast level, but the overall large-scale gradients in the background light have been removed.

For most visits, the area between galaxies is much larger than that occupied by galaxies and the catalogs can be considered effectively complete to the same level except in the close vicinity of cluster galaxies. The one exception is Visit 19, which contains NGC 4874 and many other ellipticals in the cluster core (Figure 1(a)). This pointing is nearly entirely dominated by the light from one galaxy or another; it is also the one with the highest concentration of GCs. To address this, we implemented an iterative galaxy subtraction algorithm that produced a fully background subtracted image (Figure 1(b)).

We subtracted the 10 brightest galaxies from Visit 19. We started from the brightest (NGC 4874 itself) and worked to the faintest of the ten. In each case, we first manually masked all the bright galaxies except for the one being subtracted. We then used the IRAF `ellipse` and `bmodel` tasks (Jedrzejewski 1987) to model the isophotes of the object galaxy. Because the `ellipse` fitting only occurs out to a finite radius, the resulting model will have finite extent and the subsequent subtraction will leave a sharp discontinuity in the image. For convenience of object detection, we extended the `ellipse`-generated models with a power-law fit to the last five data points in the profile at fixed ellipticity. This allowed for a smooth subtraction out to the borders of the ACS image. After subtracting one galaxy, we then repeated the process with the next brightest galaxy on the subtracted image. After the last galaxy was subtracted, we used Source Extractor to create and subtract a background map that removed large scale variations. This last step is important because it allows us to recover from any large scale over- or under-subtractions due to mismatches between the power-law extensions and the true surface brightness profiles of the galaxy. A similar technique was used with success by Jordán et al. (2004) in ACS images of Virgo cluster galaxies, although that was only for single galaxies.

After galaxy subtraction, we generated catalogs with Source Extractor, using variance maps that accounted for the extra Poisson noise expected from the subtracted galaxy light. These catalogs contain objects much closer to the centers of galaxies, and to NGC 4874 in particular. Photometry was obtained by using 3 pixel radius (0.″15) circular apertures with aperture corrections and zero points from Sirianni et al. (2005). Unless otherwise specified, all magnitudes in this paper are on the AB system. These objects are included in the DR2 catalogs of Hammer et al. (2010).

2.3. Completeness

We use artificial star tests to quantify the spatially varying detection efficiency across our images. This is particularly important for the galaxy-subtracted image containing NGC 4874, where the bright galaxy light affects the depth of our observations.

We first use routines in DAOPHOT II (Stetson 1987) to construct an empirical point-spread function (PSF) using bright point sources in Visit 19. At the distance of the Coma cluster, nearly all globular clusters are unresolved with *HST* and can be well approximated by point sources (the mean half-light radius of GCs, $r_h \approx 3$ pc, is only ∼6% the full width at half-maximum of the PSF). Because detection is done only in the F814W band, we only add artificial stars to these images.

When adding point sources into the images, we avoid objects in the image as well as artificial stars already placed so as to avoid incompleteness due to confusion. We run the exact same detection pipeline on these images as we do to create our object catalog and record whether the objects were detected as a function of magnitude and position. The number of artificial stars added and measured—7,000,000 in Visit 19 alone and approximately 4240 arcmin^{-2} for the other visits—ensures that we can derive a completeness curve for any position in the survey and for any GC selection criteria.

In a typical blank area in our images observed with the full exposure time, the 90% completeness level is at $I \approx 26.8$ mag, and the 50% completeness level is at $I \approx 27.3$ mag. At $R \approx 2'$ from the center of NGC 4874, however, these limits are 1.5 mag shallower.

2.4. Globular Cluster Candidate Selection

One of the main benefits of GC studies with *HST* is the ability to use morphology and resolution to separate GCs from their main contaminants, background galaxies. At Coma distances, GCs are point sources when observed with *HST*, but the great

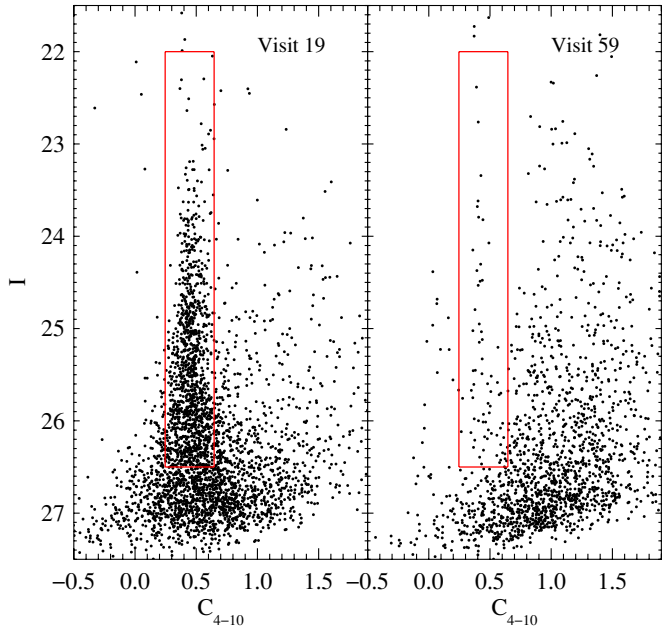

Figure 2. I magnitude vs. concentration index ($C_{4-10} = m_{4\mathrm{pix}} - m_{10\mathrm{pix}}$) for Visit 19, the central pointing containing NGC 4874 (left) and Visit 59, the background pointing most distant from the cluster center which contains mostly background galaxies (right). The vertical locus of points around $C_{4-10} = 0.45$ contains point sources. Most of the point sources in Visit 19 are likely to be GCs. The background galaxies are mostly resolved to be more extended than the GCs until $I \sim 27$, where some overlap the stellar locus. The red outlines shows our selection region for GCs.

(A color version of this figure is available in the online journal.)

majority of background galaxies are resolved. We use this ability to select against background contaminants and produce a relatively clean sample of GC candidates.

We use a rough but effective concentration criterion to select GCs. Figure 2 shows the "magnitude-concentration" diagram for objects, where we measure a concentration index, C_{4-10} using the difference in magnitude measured in a 4 pixel diameter aperture and a 10 pixel diameter aperture. Figure 2 shows that this index works well to distinguish point sources from extended sources. Here, we show the distribution of objects in Visit 19 (the one containing NGC 4874), which has the largest number of GC candidates. We overplot the objects from Visit 59, which is the most remote of our fields and contains mostly background galaxies. The red lines show our selection region where we exclude nearly all of the background galaxies. Although we experimented with different cuts in this diagram, including a variable width of the selection region with magnitude, the variations were not significant and we decided in the end that simplicity was best, choosing a cut of ± 0.2 mag around the median concentration for point sources ($\langle C_{4-10} \rangle = 0.45$).

For the purposes of this study, we wish to maximize the number of good GC candidates, while also balancing the increasing number of background contaminants with magnitude. Because of the depth and high spatial resolution of our data, we chose a fairly conservative magnitude limit, including objects with $I < 26.5$ mag. At this magnitude, our data is 97% complete in regions free of galaxy light, so completeness corrections are only important toward the centers of galaxies. At the Coma cluster distance ($m-M = 35$), assuming an extinction $A_I = 0.017$ mag for NGC 4874 (Schlegel et al. 1998), this limit should include a significant fraction of the GCs in a Gaussian GC luminosity function (GCLF) typical of giant ellipticals. We use the recently measured I-band GCLF measurement for the Virgo cD galaxy M87 (Peng et al. 2009), which was performed with deep *HST*/ACS observations in the same F814W filter used by the ACS Coma Survey. Peng et al. (2009) quote a GCLF Gaussian mean and sigma of $\mu_{I,\mathrm{Vega}} = -8.56$ mag and $\sigma = 1.37$ mag. For AB magnitudes, we add 0.436 mag to $\mu_{I,\mathrm{Vega}}$ (Sirianni et al. 2005). Assuming these values for a Gaussian GCLF, our GC catalog magnitude limit should include ∼39% of all GCs and ∼75% of the luminosity in GCs.

This is likely an oversimplification, however, as both the mean and width of the GCLF is known to vary with galaxy mass (Jordán et al. 2006, 2007). If we assume a Gaussian GCLF typical of dwarf ellipticals in clusters ($\mu_{I,\mathrm{Vega}} = -8.1$ mag and $\sigma = 1.1$ mag; Miller & Lotz 2007), then our limit includes ∼22% of the total number. This discrepancy is one of the main systematic uncertainties in our analysis. We emphasize, however, that changing the assumed GCLF does not affect the significance of our result, just the inferred total number of GCs. Given that the depth of our data is not sufficient to measure the GCLF parameters directly, we choose to assume the brighter GCLF, seen in giant ellipticals, as this will give us a lower estimate for the number of GCs in any given area. The numbers could be higher by ∼80% in regions where the GCLF for dwarf ellipticals is more representative.

We also introduce a broad color cut of $0.6 < (g - I) < 1.5$ that should include all old globular clusters. This color range is based on the transformed g–z colors of GCs in the ACS Virgo Cluster Survey (ACSVCS; Côté et al. 2004; Peng et al. 2006) and mainly eliminates distant, compact red galaxies. The ages of extragalactic GCs across all metallicities are primarily old (> 5 Gyr), especially those associated with massive early-type galaxies (e.g., Peng et al. 2004; Puzia et al. 2005; Beasley et al. 2008; Woodley et al. 2010), so this color range should include all bona fide GCs.

3. SPATIAL DISTRIBUTION OF GC CANDIDATES

Figure 3 plots the locations of GC candidates in our ACS images on a DSS image of the cluster. While it is not surprising that the number of GCs is high around massive ellipticals such as NGC 4874, what is striking about this figure is that the number of GCs across the *entire* central mosaic is high and is significantly elevated when compared to the numbers in the outer fields. Even the corner fields of the central mosaic have many more GCs. Of the six outer fields, three in the southwest (lower right) have visibly elevated GC numbers due to their proximity to NGC 4839 (top) and NGC 4827, two giant early-type galaxies. The three other fields to the south are not near massive cluster members. We take these three southern fields as an upper limit on the background contamination from foreground stars and compact distant galaxies. All of these fields have fewer GC candidates than does any field in the central mosaic.

Other than an obvious concentration around NGC 4874 and NGC 4889 (the latter of which was not observed with ACS), the GC distribution is relatively uniform across most of the central mosaic and not spatially clustered, i.e., with the exception of the two central ellipticals, the spatial structure of the GCs is not highly correlated with the positions of cluster galaxies. This is partly a bias introduced by the failure of Source Extractor to detect GCs that are immediately in the vicinity of bright galaxies. However, GC detection should not be a problem in the halos of the galaxies, and except in a few cases we do not detect the kind of small-scale substructure one would expect in

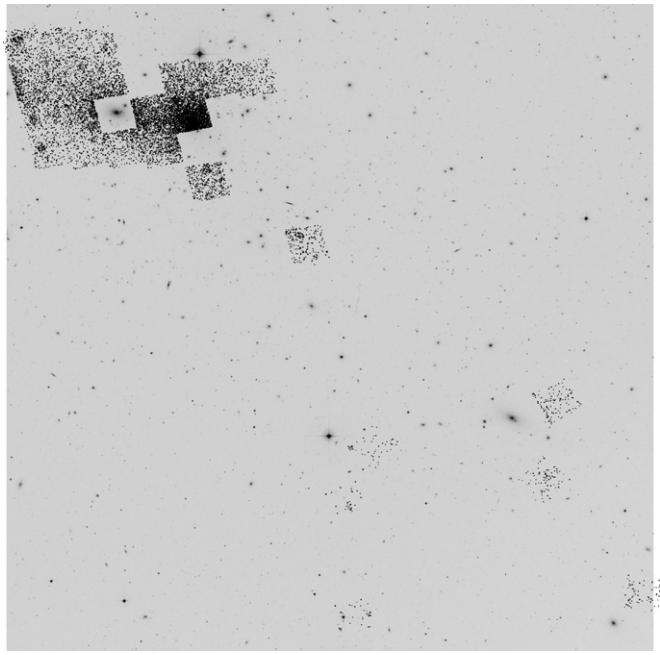

Figure 3. Spatial distribution of ACS GC candidates shown on a $1^\circ \times 1^\circ$ Digitized Sky Survey image of the Coma cluster with north up and east to the left (1.75×1.75 Mpc at Coma distance). At the top left of the image is the observed portions of the cluster core central mosaic. The largest concentration of GCs is around the central galaxy, NGC 4874. The other large galaxy, unobserved by ACS, is NGC 4889. At the bottom of the image are six fields in the outer regions of the cluster. The three outer fields to the right (west) show higher numbers of GC candidates because of their proximity to large galaxies. The eastern three outer fields (bottom center) are not near large galaxies and are used as background fields. The density of GC candidates throughout the entire cluster core is much higher than in the background regions, implying a large population of intracluster GCs. The ACS field sizes are roughly $202''$ on a side.

the cluster GC distribution if all the GCs were tightly associated with galaxies.

Figure 4 shows more clearly the distribution of GCs in the cluster core. To produce this figure, we divide the core region into $20'' \times 20''$ "pixels" with each representing the surface density of GCs, corrected for spatially varying completeness, and smoothed with a Gaussian kernel with $\sigma = 30''$. The large concentration of GCs at the center right is the GC system of NGC 4874. The GC system of NGC 4889 is also evident, although the galaxy itself was not observed. While Figure 3 shows that the overall surface density of GCs is well above the background, Figure 4 shows hints of large-scale substructure in the GC spatial distribution. There appears to be an extended structure of IGCs connecting NGC 4874 to NGC 4889 to NGC 4908 and IC 4051, both of which lie just beyond the eastern edge of the mosaic.

These observations suggest the existence of a large intergalactic population of globular clusters. In the following sections, we seek to verify and quantify their existence.

4. BACKGROUND ESTIMATION AND GALAXY MASKING

Contaminants to our sample of GCs consists of foreground stars and faint, unresolved background galaxies (the sum of which we generically refer to as "background"). This background is important to quantify, as a smooth background can mimic a smooth IGC population. Ground-based IGC studies in Coma are typically plagued by high background due to their inability to distinguish distant galaxies from point sources.

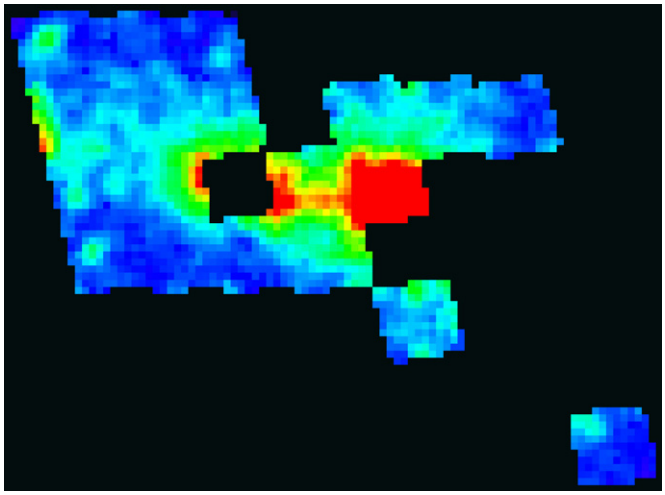

Figure 4. Smoothed spatial distribution of GCs in the Coma cluster core ($30.'8 \times 23.'0$, 900×670 kpc). Pixels are $20''$ on a side, and color represents the surface density of GCs, corrected for completeness (blue–red denotes low–high density). The entire image has been smoothed by a Gaussian kernel with $\sigma = 30''$. The dominant concentration of GCs is around NGC 4874 and an extended structure of GCs appears to connect NGC 4874, 4889, and 4908. Some peaks in the distribution represent individual cluster galaxies.

(A color version of this figure is available in the online journal.)

As a measure of our background, we choose the three outer ACS fields—visits 45, 46, and 59—that are not near giant galaxies, and are shown at the bottom center of Figure 3. For each of these fields, we select GC candidates as described earlier and also mask the regions containing a few obvious Coma members using the prescriptions described below. The surface density of GC candidates over these three fields is 2.8 ± 0.3 arcmin^{-2}, or $\sim$28 per ACS field. As we will show, this is nearly an order of magnitude lower than the density of GCs even in the outer fields of the Coma core.

To verify this background level, we compared our point source counts in these fields to those in the COSMOS *HST* Treasury project (Scoville et al. 2007). The COSMOS survey imaged 1.8 deg^2 at high Galactic latitude with the same camera (ACS/WFC), filter (F814W), and depth as the Coma Cluster Survey. The number of point sources in our three background fields is entirely consistent with the numbers expected from the surface density of stars in the COSMOS fields. Down to $I_{814} < 25$ mag, we detect 104 ± 10 point sources in our three background fields and 98 are expected using the average surface density from the COSMOS data. This independent check gives us more confidence that our background value is correct.

The fact that the global background is so low compared to the detections in our Coma core fields gives us confidence that we are indeed detecting GCs within the Coma cluster. The more difficult question is whether these objects are truly "intergalactic" or simply part of extended galactic systems. This debate is not one easily resolved by imaging data alone. We can, however, address the contribution from galactic GC systems in two ways. First, we aggressively mask regions around known bright galaxies. Second, we can make certain assumptions about the numbers and spatial extent of the GC systems of observed cluster members and compare simulated GC distributions to the observations. We do this in order to test the hypothesis that the GCs observed in the cluster core are an intergalactic population.

The details of these two methods are described in Appendix A. In short, we generate masks around all galaxies

with luminosities down to $M_g < -17$ mag, both in and around all of our fields. The detection algorithm that we use for GCs actually ends up masking GCs around fainter galaxies because our chosen background estimation parameters cannot follow the steeply rising surface brightness profiles at the centers of galaxies. For each galaxy, we apply a liberal, size-dependent mask to the surrounding regions. These masks should eliminate ∼90% of the "galactic" GCs from our catalogs. For the remaining outer GCs, we subtracted a model GC system using an assumed Sérsic $n = 2$ profile for the GC surface density, a reasonable assumption given previous measurements of GC system radial profiles. The parameters of this model are estimated based on scaling relations for S_N and R_e from Peng et al. (2008; E. W. Peng et al. 2011, in preparation). This modeling is done for all Coma galaxies in the Eisenhardt et al. (2007) catalog, which is complete to $M_V < -16$ mag and extends to $M_V < -14$ mag. This is described in greater detail in Appendix A.2.

Although we have taken great pains to model and subtract any residual GCs that may belong to Coma galaxies, we find that our final result is largely insensitive to the assumed parameters. The detection of IGCs, as we will show below, is highly significant and not dependent on the details of the background or the modeling of GC systems. We estimate the systematic uncertainty due to our modeling procedure to be $^{+4000}_{-5000}$ GCs (Appendix A.3), only 5%–9% of the inferred IGC population.

5. RESULTS

5.1. Radial Profile of GCs in the Coma Cluster

NGC 4874 has previously been observed to have a large number of globular clusters (Blakeslee & Tonry 1995; Harris et al. 2000, 2009). It has also been shown to have a GC system whose spatial profile is shallower and more extended than those for other elliptical galaxies (Harris et al. 2009). Could the GCs that we see filling the cluster core simply be the extended GC system of NGC 4874? The situation is complicated by the fact that the core of the cluster contains not one but two giant ellipticals, the other being NGC 4889, as well as many other member galaxies.

In Figure 5, we show the radial distribution of GCs in the cluster core, centered on NGC 4874. For each bin in radius, we sum up the number of observed GC candidates in unmasked regions, subtract the expected contribution of GCs from other Coma galaxies (shown as the dotted line in Figure 5), and subtract the global background level (dot-dashed line), leaving what should be the NGC 4874 and IGC population. We determine the mean completeness of the sample within the annulus and extrapolate the total number of GCs assuming the M87 GCLF as described above. We then sum the total observed, unmasked area within the annulus to determine the surface number density of GCs. The random errors in each bin are derived from the Poisson errors for the number of candidate GCs as well as from the Poisson error in the background, added in quadrature.

This profile, tabulated in Table 1, represents our best estimate of the radial surface density distribution of the GC system surrounding NGC 4874, uncontaminated by the GC systems of other cluster members. Perhaps the most interesting feature of this profile is a marked inflection at $R \sim 200$ kpc, beyond which the GC surface number density decreases much more slowly with radius. We interpret this flattening of the profile as the region where a large and extended population of IGCs starts to dominate the GCs directly associated with NGC 4874.

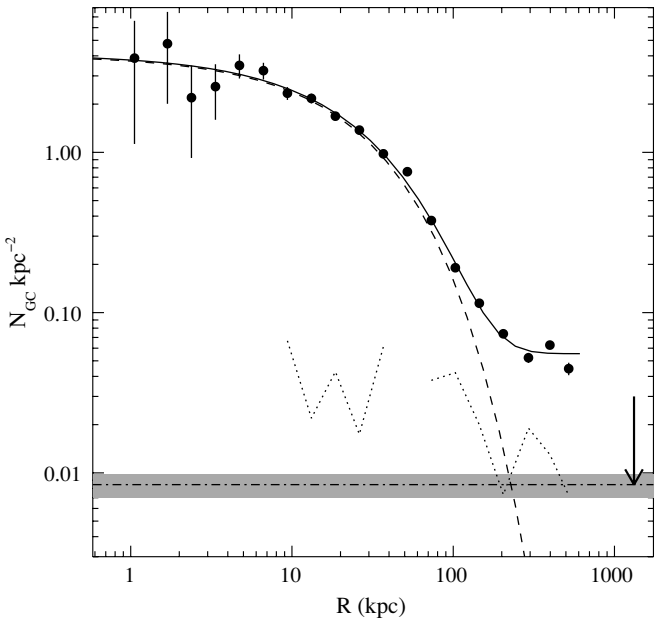

Figure 5. Radial distribution of GCs in the Coma cluster core centered on NGC 4874. The surface density of GCs in each bin (black points) is calculated after masking around known galaxies and statistical subtraction of GCs belonging to these cluster members. The radial profile exhibits a flat inner core as well as an inflection and flattening at large radii. We interpret the flat distribution at large radii as evidence of a large population of IGCs. The dot-dashed line and gray band at bottom denote the surface density of background objects (plus 1σ errors) determined from our outer ACS fields and subtracted from all radial bins. The background level is a factor ∼7 below that in the outermost bins. The arrow at bottom right shows the mean distance of the three background fields from NGC 4874. The dotted line is the modeled radial distribution of GCs belonging to cluster members that are still visible after masking. These have been subtracted from the GC radial profile, although they too are well below the overall level by a factor of a few. The data are well fit by a Sérsic model plus a constant level (solid line). The Sérsic component alone is shown as the dashed line.

The significance of this detection is extremely high, as the background level is shown in Figure 5 by the horizontal dot-dashed line at the bottom, with the estimated error of the background denoted as the shaded gray region. The inferred IGC surface density is a factor ∼7 over the background. Another point of comparison is with the modeled surface density of remaining unmasked galactic GCs, shown as the dotted line, which also has already been subtracted from our total GC profile. The overall surface density of GCs in this cluster profile is well above the surface density of masked galactic GCs (by a factor 4–7), and thus the GCs we see are likely to be truly intergalactic. We have also found that our results do not change significantly if we only use data from the eastern or western half of the Coma core.

A single Sérsic profile, normally a good fit to the surface density profiles of GC systems, is not sufficient to describe the data for the central Coma cluster GCs. Instead, we fit a model combining a Sérsic profile and a constant. It is likely that the IGCs have a radially decreasing density profile (although the simulations of Bekki & Yahagi 2006 suggest that they can also have a flat density distribution within the central few hundred kiloparsecs), but the data only allow us to measure their mean surface density. The solid line in Figure 5 traces the best-fit model, and the dashed line that follows it until large radii is the best-fit Sérsic component. The fitted surface density of IGCs is 0.055 ± 0.002 kpc^{-2}, which is a 19σ detection over

Table 1
GC Radial Surface Density Profile Centered on NGC 4874

$\langle R \rangle$ (arcmin)	σ (arcmin^{-2})	Area (arcmin^2)
0.036	3276 ± 2321	0.00546
0.058	4031 ± 2331	0.00719
0.082	1856 ± 1076	0.01428
0.115	2175 ± 825	0.02834
0.162	2950 ± 507	0.05617
0.229	2737 ± 326	0.11152
0.322	1978 ± 181	0.22114
0.454	1837 ± 128	0.38152
0.639	1423 ± 91	0.56911
0.900	1164 ± 71	0.73770
1.268	828 ± 52	0.96299
1.786	641 ± 39	1.45523
2.516	318 ± 15	4.62493
3.543	161 ± 7	12.59246
4.991	97 ± 4	22.04740
7.030	62 ± 4	16.82656
10.066	44 ± 3	19.62118
13.674	53 ± 2	40.98172
17.886	38 ± 3	14.17776

Notes. These surface densities are corrected for completeness, the full Gaussian GCLF, and include the masking and subtracting of GCs belonging to other cluster members, as described in Section 5.1. The surface density of contaminants (also correcting for the GCLF) as marked by the dot-dashed line in Figure 5 is 7.2 ± 1.2.

the background, 0.00845 ± 0.001 kpc^{-2}, assuming Poisson random errors. As we discuss in Section 4 and Appendix A.3, we also need to account for systematic uncertainties from our modeling, but they do not affect the main conclusion, which is high significance of the detection. We list the best-fit parameters in Table 2.

Although we cannot determine the shape of the IGC component's density profile, one constraint is that it must fall rapidly after the limits of our data. The mean distance of the three fields we are using to measure the background is shown as the vertical arrow at 1.3 Mpc. Therefore, the GC surface density must fall to zero, or at least the level of the dashed line, by this distance. A steep falloff like this favors a low n Sérsic profile for the IGCs (n = 1–2), similar to the ICL profiles in Seigar et al. (2007) and X-ray gas in galaxy clusters (Demarco et al. 2003), but lower (i.e., steeper in the outer regions) than dark matter halo density profiles (Merritt et al. 2006). However, at these radii, it may not make as much sense to speak of a circularly symmetric GC radial profile and it would be more useful to map in two dimensions the spatial distribution of GCs.

5.2. Total Numbers of GCs and Specific Frequency

We use our radial spatial density profile to estimate the total number of GCs in the cluster core, which we define to be the extent of our data. Integrating this profile for $R < 520$ kpc gives a remarkable 70000 ± 1300 GCs, with the IGC component dominating the GC population beyond 150 kpc. As listed in Table 2, the number of GCs belonging to NGC 4874's "Sérsic component" out to this radius is ≈23,000, leaving a remaining 47,000 ± 1600 (random) $^{+4000}_{-5000}$ (systematic) to be IGCs. There are over *twice* as many IGCs as there are GCs from the Sérsic component, resulting in an IGC fraction of the entire central GC system of ∼70%.

With a measurement of NGC 4874's luminosity, we can calculate an "intrinsic" specific frequency for the galaxy. Harris et al. (2009) use a luminosity of $M_V = -23.46$ (adjusted to $D = 100$ Mpc), but surface brightness profiles from SDSS imaging (J. Lucey 2010, private communication) and KPNO 4 m CCD imaging (R. Marzke 2010, private communication) show the galaxy to be substantially brighter. Measurements of the total r-band luminosity from mosaicked SDSS frames gives a value of $r = 10.23$ ($M_r = -24.77$, assuming $E(B-V) = 0.009$ from Schlegel et al. 1998), which includes a 0.32 mag extrapolation using the best-fit Sérsic profile for the light beyond $R = 7'$. The mean color of the galaxy is $g - r \approx 0.8$ mag, which produces $M_V = -24.47$ using the Lupton 2005 transformation derived by matching SDSS photometry to Peter Stetson's published photometry for stars.[23]

Table 2
Best Parameters for Sérsic Plus Constant ($\Sigma_{\rm IGC}$) Model Fit to Coma Central GC System

Parameter	Value	Description
n	1.3 ± 0.1	Sérsic index
R_e	62 ± 2 kpc	Sérsic effective radius
Σ_e	0.437 ± 0.034 kpc^{-2}	GC surface density at R_e
$\Sigma_{\rm IGC}$	0.055 ± 0.002 kpc^{-2}	Mean IGC surface density
$N_{\rm GC,tot}$	70000 ± 1300	Total GCs within 520 kpc
$N_{\rm GC}$, Sérsic	23000 ± 700	"Sérsic" GCs within 520 kpc
$N_{\rm IGC}$	47000 ± 1600 (r) $^{+4000}_{-5000}$ (s)	IGCs within 520 kpc

With this, we calculate an "intrinsic" specific frequency for NGC 4874 of $S_N = 3.7 \pm 0.1$ (the errors are purely from the total numbers of GCs and do not include errors in the luminosity).[24] This value is very much in line with the those of non-cD, giant early-type galaxies in the Virgo and Fornax clusters.

If we assume that all GCs (including IGCs) are part of the NGC 4874 system and that we are not missing any luminosity from the galaxy, then this would give the specific frequency within 520 kpc a higher value of $S_N = 11.4 \pm 0.2$, a value similar to those measured for some cD galaxies. Another interpretation, which we discuss later, is that the specific frequency of the system is the lower, more normal value, but that the IGCs are tracing a large amount of intracluster starlight that is unaccounted for.

5.3. Comparison to NGC 4874 Surface Brightness Profile

A relevant comparison for the GCs is to the surface brightness profile of the field starlight of NGC 4874. In Figure 6, we plot the light profile in circular apertures around NGC 4874 from two independent data sets (with arbitrary normalization). As mentioned in the previous section, the first is from measurements using SDSS r-band imaging (J. Lucey 2011, in preparation) and the second uses imaging from the Mosaic-I camera on the KPNO 4 m telescope (R. Marzke 2010, private communication). Both profiles are in good agreement in the inner regions ($R < 20$ kpc), but start to diverge in the outer regions due to differences in the sky measurements. The difference between the two profiles is at the level of 2% of the sky.

In the regions beyond 100 kpc, we also plot the surface brightness profile of the "intracluster background light" in the Coma cluster as determined photographically by Thuan &

[23] http://www.sdss.org/dr7/algorithms/sdssUBVRITransform.html#Lupton2005

[24] If we use the older, fainter value for the luminosity, then $S_N = 9.5 \pm 0.3$, which is consistent with the value found in the *HST*/WFPC2 study of Harris et al. (2009). Their data only extended to $R \sim 65$ kpc and thus were not able to detect the IGC population. The higher value is also consistent with the value estimated by Blakeslee et al. (1997), who also used a fainter luminosity.

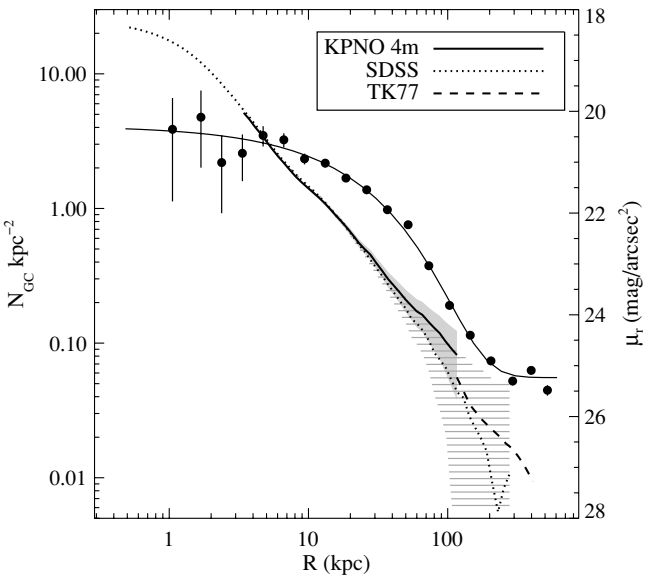

Figure 6. Radial distribution of GCs centered on NGC 4874 (black dots) compared to the surface brightness profile of field starlight around NGC 4874. Three different sources are used for the surface brightness profiles: KPNO (solid), SDSS (dotted), and Thuan & Kormendy (1977, dashed). The shaded and striped regions represent a change in sky determination of ±2% for the KPNO and SDSS profiles, respectively. The GC radial surface number density profile and the field star surface brightness profile do not exhibit similar shapes at either small or large radii. The surface brightness measurements at large radii, however, are entirely dependent on an accurate measure of the sky brightness.

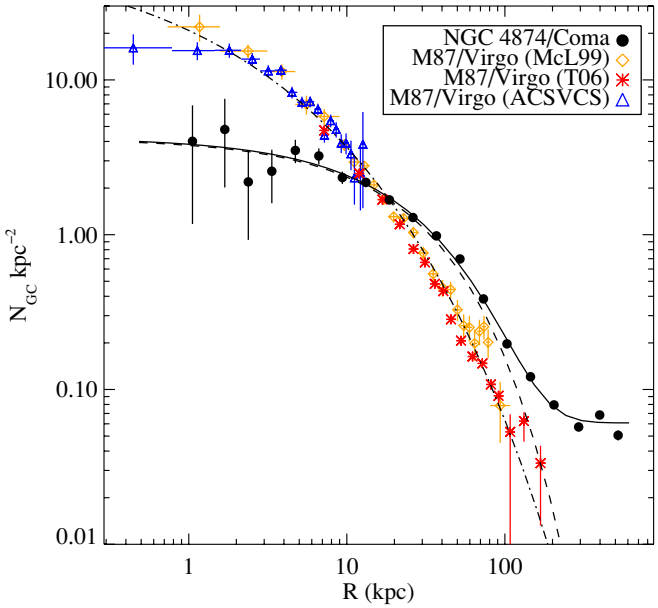

Figure 7. Radial distribution of GCs centered on NGC 4874 (black dots) compared to the distribution of GCs around the Virgo cD galaxy M87. M87 data is from McLaughlin (1999, McL99, orange diamonds), Tamura et al. (2006, T06, red asterisks), and the ACS Virgo Cluster Survey (Peng et al. 2008; blue triangles) with a Sérsic fit to the combined data set overplotted (dot-dashed). The Coma GCs have a much shallower and larger core, as well as an inflection where IGCs begin to dominate. Even with the larger T06 data set, there is no evidence yet for a profile inflection around M87 like what we see in Coma, although the data do not go comparably far out in radii.

(A color version of this figure is available in the online journal.)

Kormendy (1977), transforming from $\mathcal{G}$ to r magnitudes using an offset of $(\mathcal{G}-r) = 0.37$ mag, based on a $(B-V) = 0.7$ mag, their published transformation from $\mathcal{G}$ to Thuan–Gunn r (Thuan & Gunn 1976), and then an offset to SDSS r (Fukugita et al. 1995). This profile appears to match the SDSS photometry at $R \sim 100$ kpc but then continues with a shallower slope.

It is clear that at large radii ($R > 100$ kpc), the determination of the sky is crucial to the measurement of the ICL. To illustrate this, we shade in the regions corresponding to a change in sky determination of ±2% of the sky level around the KPNO and SDSS measured profiles. Although there is no evidence for a "break" in the measured surface brightness profiles akin to what we see in the GCs, the surface brightness profile in the regions where IGCs dominate GC counts is entirely dependent on the determination of the sky level to better than 1% and thus is difficult to quantify.

We can use these profiles to calculate the "local" specific frequency of the outer GCs, although any calculation is highly uncertain due to sky subtraction for the surface photometry. Nevertheless, we can take these surface brightness profiles at face value to see if the calculated values are reasonable. Assuming that the surface brightness at $R = 200$ kpc is $\mu_r \approx 26.2$ mag (following the Thuan & Kormendy profile) and using $V - r = 0.2$ mag for old metal-poor stellar populations, then $\mu_V(200\ \mathrm{kpc}) \approx 26.4$ mag. Given the IGC surface density at these radii (46 arcmin^{-2}), we estimate $S_N(200\ \mathrm{kpc}) = 5$. If we assume the profile derived from SDSS data, however, then $\mu_V(200\ \mathrm{kpc}) \approx 27.5$ mag, resulting in $S_N(200\ \mathrm{kpc}) = 13$. We emphasize that the surface photometry is extremely uncertain at these radii and the upper error bar on this number is essentially unconstrained. The local values of S_N at these kinds of radii have previously been reported to be quite high (Tamura et al. 2006 in M87 and Rhode & Zepf 2001 for NGC 4472), but those measurements are equally uncertain for similar reasons.

In the inner regions, there is a notable divergence between the GCs and the galaxy light. The galaxy does not show the prominent core within 10 kpc that the GC system does, only displaying a flattening in the profile at a smaller radius.

5.4. Comparison to the M87 GC System

Perhaps the most relevant local comparison for the NGC 4874/Coma cluster GC system is that of M87 in the Virgo cluster. In Figure 7, we show the GC radial surface density profiles of the two GC systems. The outer M87 profile is taken from the data of McLaughlin (1999) and Tamura et al. (2006), while the central regions of the profile are from the ACSVCS data shown in Peng et al. (2008). We note that the physical resolution of the Coma *HST* data is very competitive with ground-based Virgo observations (0.″1 resolution at Coma distance is equivalent to 0.″6 resolution at Virgo distance), but obviously cannot match the ACSVCS observations of M87. None of the Virgo data sets go as far out in physical radius as our Coma data, but they still provide a useful comparison. The two GC systems profiles are similar in the range of intermediate radii (20–100 kpc), but differences appear in the very inner and outer regions. Most noticeably, the Coma GC systems display a very pronounced core within 10 kpc, which does not appear to be present in the Virgo system except perhaps within 1 kpc. This deficit of GCs at the center of NGC 4874 is also evident in the analysis of Harris et al. (2009). This core could be the result of dynamical friction destroying GCs at the center of NGC 4874.

The core in the GC profile, and the divergence from the M87 GC profile, is most evident within 10 kpc. Could this be due to unaccounted observational incompleteness? The four innermost radial bins ($R < 3.5$ kpc) have the largest errors and shallowest observations because of the bright galaxy light (completeness of

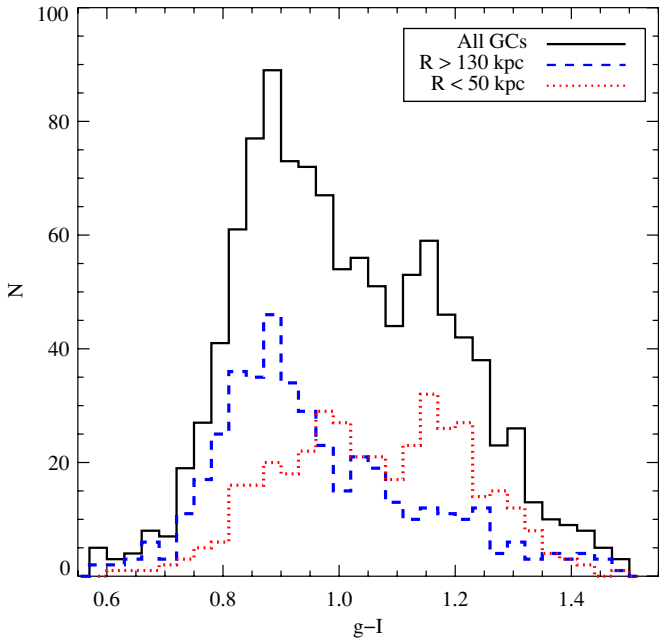

Figure 8. Color distributions of all GC candidates in unmasked regions with $I < 25$ (black solid line), a predominantly IGC subsample with $R > 130$ kpc (blue dashed line), and a predominantly galactic GC subsample with $R < 50$ kpc (red dotted line). The total distribution exhibits a bimodality typical for extragalactic GC systems, as does the IGC sample. For the IGCs, blue GCs outnumber red GCs by a ratio of 4:1. Only in the inner regions, where the GC system of NGC 4874 is dominant, does the number of red GCs compare to the number of blue GCs. The color distribution of the inner GCs is also bimodal, but with the blue population having a much redder color.

(A color version of this figure is available in the online journal.)

the GCLF is $\approx 25\%$ in these bins). There are multiple reasons, however, why we believe these lower surface densities to be real. The radius at which the core becomes apparent, 20″, is large for *HST* imaging. Even excluding the inner 10″ (4.8 kpc), the difference in slope between the two GC profiles is still apparent. Also, the completeness tests we apply also take into account incompleteness due to imperfect profile subtraction and thus is a true measure of the completeness in these radial annuli. In order to turn the M87 GC profile into the Coma GC profile through a systematic overestimation of the completeness, the completeness would have to be overestimated by nearly an order of magnitude. Lastly, this deficit of GCs relative to the galaxy light profile was also independently found by Harris et al. (2009) using *HST*/WFPC2 data (see their Figure 6).

In the outer regions the M87 profile follows the single-Sérsic fit out to the limits of the data. The Virgo data, however, only reaches a radius of 130 kpc, and thus would not be sensitive to the kind of IGC population we see in Coma. In fact, if the Coma data had the same physical radial extent, it would have been very difficult to detect the IGC population. More deep, wide-field imaging of the area around M87, such as the Next Generation Virgo Survey,[25] will be necessary to detect or place more stringent limits on a population of IGCs in Virgo.

5.5. GC Color Distributions

For old GCs, the broadband color is an indicator of metallicity. The color distributions of extragalactic GC systems have been studied extensively with *HST* (e.g., Larsen et al. 2001; Peng et al. 2006) and are often bimodal in nature (Gebhardt & Kissler-Patig 1999), especially in massive early-type galaxies. In Figure 8, we plot the color distribution of bright GCs (applying a magnitude limit of $g < 25$ mag for higher signal-to-noise ratio (S/N)) in the unmasked regions of the Coma cluster core. The color distribution of all GCs shows the typical bimodality seen in extragalactic GC systems, displaying a prominent peak of blue (metal-poor) GCs with $(g - I) \approx 0.9$ and a red (metal-rich) peak with $(g - I) \approx 1.15$.

We plot the color distributions divided by distance from the center of NGC 4874—those within 50 kpc (galactic GCs) and those outside of 130 kpc (predominantly IGCs). We use the Kaye's Mixture Model (KMM; McLachlan & Basford 1988; Ashman et al. 1994) implementation of the expectation-maximization (EM) method to fit two Gaussians with the same standard deviation to the GC color distributions of each sample. Both the galactic and intergalactic GCs are much better described by bimodal distributions in color than by a single Gaussian with p-values less than 0.001. The inner blue GCs, however, have a much redder mean color—$(g - I) = 0.94$ as opposed to $(g - I) = 0.89$ for GCs in the outer regions—such that they are nearly merged with the red GCs $(g - I) = 1.18$. The metal-poor GCs are either quite red or there is a substantial population of GCs at intermediate color. It could also be the sign of a significant radial color gradient within the blue GC subpopulation (e.g., Harris 2009; Liu et al. 2011). This gradient could be in metallicity or in age, reminiscent of younger metal-poor GCs in Local Volume dIrr galaxies (Sharina et al. 2005; Georgiev et al. 2008, 2009), although the colors of the blue GCs are not so blue as to require very young ages. The inner regions also have equal numbers of blue and red GCs where the fraction of red GCs is $f_{\rm red} = 0.51$.

The generally red colors of the inner GCs was noted by Harris et al. (2009), who used their WFPC2 data to show that the inner regions of the GC system had a high ($\gtrsim 50\%$) fraction of red GCs. Using the larger ACS coverage of our survey, however, we see that the total GC system around NGC 4874 is dominated by blue GCs. In the outer sample plotted in Figure 8, the IGC population is dominated by blue GCs with a blue-to-red ratio of 4:1, ($f_{\rm red} = 0.2$) although the fraction of red GCs is still significant. Even measuring only the Sérsic component of the GC subpopulations, the NGC 4874 GCs are dominated by blue GCs, with the red GCs being more spatially concentrated. The radius at which the surface density of blue and red GCs are equal is $R \approx 40$ kpc. Thus, like the giant ellipticals in the Virgo cluster (Peng et al. 2008), the GC system of NGC 4874 as well as the IGC population, is dominated by blue GCs.

The mean colors of the blue and red outer GCs are $(g - I) = 0.89$ and 1.22, respectively. The blue peak has a typical color for the GC systems of galaxies with masses at or below L^* (Peng et al. 2006). The red peak, however, is still fairly red, having nearly the same mean color as the inner GCs around NGC 4874. We caution that some of these red GCs may be from the large metal-rich GC system of NGC 4889 and other more massive cluster members.

We can do a simple test to see if the red GCs beyond 130 kpc are associated with luminous galaxies. We calculate the distance from each GC to the nearest luminous ($M_B < -17$) galaxy and compare the mean shortest distance for the red and blue GCs. We find that there is no significant difference between these two populations. The median shortest distance for red GCs is 75″ and that for blue GCs is 74″, with the biweight Gaussian sigmas of each distribution being 35″. The spatial behavior of the red

[25] The Next Generation Virgo Survey (NGVS) is a Large Program with the Canada–France–Hawaii Telescope.

and blue GCs beyond 130 kpc are identical and is consistent with a population of IGCs mostly uncorrelated with nearby galaxies.

6. DISCUSSION

6.1. Intracluster Light Inferred from IGCs

The existence of intracluster starlight and globular clusters has for decades been considered important, but always difficult to observe. Recently, as observations have improved and theory has shown that intracluster stellar populations are an essential feature of galaxy–galaxy and galaxy–cluster tidal interactions, there is increased interest in quantifying its properties: total mass, spatial distribution, metallicity, and kinematics. We have shown that with *HST*, a direct detection of IGCs is a clean way to measure one component of intracluster stellar populations in nearby galaxy clusters.

Only a small fraction of the total or stellar mass is in the form of old globular clusters. The total mass fraction in GCs appears to be relatively constant across galaxies and galaxy clusters (McLaughlin 1999; Blakeslee 1999). Because of the variation in the stellar mass-to-light ratio across galaxy mass, however, the specific frequency (or stellar mass fraction) can vary widely. Massive ellipticals and dwarf galaxies can have the highest S_N, and galaxies with luminosities around L^* have the lowest S_N. The stellar mass fraction in early-type galaxies ranges from ∼0.2% to a few percent (Peng et al. 2008).

We do not know the fraction of stellar mass that is in the form of IGCs, but we can make reasonable assumptions. One possibility is that the IGCs originate from low-mass dwarf galaxies that are tidally disrupted. The S_N of such a population can vary and can depend on the clustercentric radius (Peng et al. 2008), but if we assume that dwarfs in the cluster center will have high specific frequencies, then we can reasonably assume $S_{N,\rm IGC} = 8$, which is similar to the S_N values for high-S_N dEs at the center of the Virgo cluster (Miller & Lotz 2007; Seth et al. 2004; Peng et al. 2008), the GC systems of even lower mass dwarfs (e.g., Puzia & Sharina 2008), and for Virgo cluster IGCs (Williams et al. 2007).

Such a value for the specific frequency of the IGC population would imply a total ICL luminosity within 520 kpc of $M_V = -24.4$ mag, an amount of starlight equal to the whole of NGC 4874. Spread out uniformly over this entire area, this luminosity would have a mean surface brightness of $\mu_{V,\rm ICL} = 27$ mag arcsec^{-2}, which is still challenging for surface photometry, but detectable in the best observations (Mihos et al. 2005). If we assume $M/L_V = 1.7$, a value typical of cluster dEs, then this corresponds to a stellar mass of $\mathcal{M}_{\rm ICL} \approx 9 \times 10^{11}\ \mathcal{M}_\odot$.

Assuming a lower specific frequency like $S_{N,\rm IGC} = 1.5$, as is more common for L^* early-type galaxies or low-S_N dEs and dS0s in the outskirts of the Virgo cluster, would imply a higher luminosity for the ICL. Conversely, assuming a very high specific frequency like that in M87 or the highest S_N dwarfs, $S_{N,\rm IGC} = 12$, would imply a lower ICL luminosity. The inferred ICL luminosities, surface brightnesses, masses, and central ICL fractions for these three assumed values of $S_{N,\rm IGC}$ are listed in Table 3. These values bracket the range of "local" S_N we calculate from the outer surface brightness profiles of NGC 4874 in Section 5.3. Deeper, systematically controlled photometry of the intracluster region will be the best way to set a meaningful limit on the S_N of the IGC population.

We have also calculated these values using the total luminosity in GCs, which is more robust than the total number because most of the luminosity in GCs is brighter than the mean of the GCLF (Harris 1991). Using typical values for the stellar luminosity fraction (0.2%–1.2%) from Peng et al. (2008), we arrive at very similar numbers to those in Table 3.

Table 3
ICL Luminosity, Surface Brightness, Mass, and Fraction ($R < 520$ kpc) as a Function of $S_{N,\rm IGC}$

$S_{N,\rm IGC}$	$M_{V,\rm ICL}$ (mag)	$\mu_{V,\rm ICL}$ (mag arcsec^{-2})	$\mathcal{M}_{\rm ICL}$ ($10^{11}\ \mathcal{M}_\odot$)	$\frac{\mathcal{L}_{\rm ICL}}{(\mathcal{L}_{N4874+\rm ICL})}$
1.5	−26.2	25.2	50	0.8
8	−24.4	27.0	9	0.5
12	−24.0	27.4	6	0.4

All of these inferred luminosities and masses are larger than those previously inferred from direct measurement of the low surface brightness ICL in Coma. Both Gregg & West (1998) and Adami et al. (2005) estimate a value of $M_R \approx -22$, which for an old stellar population is roughly $M_V \approx -21.5$. However, their values were the result of combining the luminosities of individual ICL sources. The 1% detection limit of the Adami et al. (2005) study is quoted as $\mu_V = 25.8$, which is much shallower than what is required if $S_{N,\rm IGC} \gtrsim 2$. It is likely that these previous studies were sensitive to overdense regions in the ICL, but not to the overall population of intracluster stars.

6.2. The Intracluster Fraction

When considering only the IGC and NGC 4874 GC system (equivalent to BCG+ICL measurements), we find that the IGCs make up ∼70% of the total "central" GC system. Although more difficult, we can also estimate the IGC fraction for *all* GCs in the cluster core, including the GCs belonging to cluster member galaxies. We do this in two ways. First, we can calculate this number only for those areas that we have observed. We assume the IGC surface density to be the fitted value in Table 2. We can subtract the surface density of IGCs from our data and what remains is the "galactic" GC population in the observed areas. Using this metric, we find that roughly ∼30% of the observed GCs belong to the intracluster population. This number does not account for the GCs close to galaxies that were missed by our detection algorithm, so it can be considered an upper limit over the area observed.

The main drawback of limiting to the observed area, however, is that we do not observe large portions of the cluster core, including the other massive elliptical, NGC 4889. Another method is to apply the GC system modeling previously described to estimate the total number of GCs within 520 kpc that belong to galaxies. When we do this, we find that the IGCs make up ∼45% of the GCs in the Coma cluster core (this fraction is higher because our observed area includes NGC 4874, depressing the IGC fraction). This number is naturally more uncertain because a large fraction of the galaxies are unobserved.

Given the assumptions in the previous section, we can infer that approximately half of the stellar luminosity associated with the "central" system (NGC 4874 and the ICL) is in the ICL. Because the ICL is likely to be more metal-poor and have a lower mass-to-light ratio than the stars at the center of NGC 4874, this translates to about one-third of the stellar mass being in the ICL. We would expect that the IGC fraction should be higher than the ICL fraction, because most of the stellar mass is in L^* galaxies that have low S_N, whereas the specific frequency of the IGC population is likely to be high. This is why we find that the IGC fraction of the "central" system is ∼70%, but that the likely ICL fractions in Table 3 are closer to 50%.

All of these numbers imply a high ICL fraction in the cluster, but are consistent with expectations from observations and simulations for the core of a massive, rich cluster such as Coma (e.g. Willman et al. 2004; Sommer-Larsen et al. 2005; Yang et al. 2009; Puchwein et al. 2010). Seigar et al. (2007) find a central ICL fraction of 60%–80% around cD galaxies, and Purcell et al. (2007) expect similar ICL fractions from simulations of tidal stripping.

Previous studies of extragalactic GC systems have also suggested that there is a roughly constant ratio between the total number or mass of GCs in a system and the total dynamical or baryonic mass (e.g., Blakeslee 1999; McLaughlin 1999; Peng et al. 2008; Spitler & Forbes 2009). If this is the case, than the IGC fraction may be more representative of the total mass fraction in the diffuse component of the galaxy cluster.

6.3. Scenarios for the Origin of IGCs

Both theory and simulations suggest that an intracluster stellar component is a natural result of many physical process that shape galaxies in the cluster environment. Galaxy–galaxy tidal interactions (e.g., Gallagher & Ostriker 1972; Moore et al. 1998; Stanghellini et al. 2006), tidal forces as galaxies orbit through the cluster gravitational potential (e.g., Merritt 1984; Gnedin 2003), tidal "preprocessing" within infalling galaxy groups (Rudick et al. 2006), tidal destruction of low mass galaxies (Lopez-Cruz et al. 1997), and tidal tails that escape from merging galaxies (e.g., Murante et al. 2007) are all plausible mechanisms to liberate stars and GCs from the gravitational potential of their host galaxy. The problem is in trying to distinguish between these mechanisms and determine what combination produces the observed intracluster stellar populations.

Based on previous ICL studies in Coma, the specific frequency of the IGC population is not likely to be very low, otherwise its associated ICL would already have been detected at relatively high S/N. One straightforward possibility is that the GCs originate mainly from disrupted dwarf galaxies, which can have high specific frequencies. Dwarf galaxies, having low masses and surface mass densities, are prone to be destroyed by interactions with other galaxies and with the cluster potential. If we assume $S_{N,\mathrm{IGC}} = 8$, then the inferred IGC population would require the disruption of ∼2300 dwarf galaxies with $M_V = -16$.

Simulations suggest, however, that the ICL originates from stars in L^* galaxies rather than from dwarfs (Willman et al. 2004; Bekki & Yahagi 2006; Purcell et al. 2007) and that a significant fraction of the ICL is first liberated in dynamically cold streams possibly thrown off from merger remnants (Rudick et al. 2009). ICL production mechanisms that depend on galaxy–galaxy interactions appear to be able to produce the right amount of intracluster mass (early calculations by Gallagher & Ostriker 1972 of stars stripped from L^* galaxies during close encounters predicted that the total ICL mass in the Coma cluster should be approximately 10^{12} $\mathcal{M}_\odot$, a number quite close to what we infer from the IGCs).

Galaxy–galaxy harassment, however, is expected to produce a more centrally concentrated IGC/ICL component than, for instance, interactions from with the mean cluster tidal field (Merritt 1984), because the cross section for galaxy–galaxy interaction is strongly peaked at the cluster center. We unfortunately cannot determine the full spatial density profile of the IGCs as our observations only reach $R = 520$ kpc. What we do measure in the IGC dominated regime ($150 < R < 520$ kpc), however, is consistent with a flat profile and shows no sign of being very centrally concentrated.

Early-type galaxies near L^* have a nearly universally low specific frequency, with $S_N \approx 2$ (Peng et al. 2008). If these kinds of galaxies were entirely disrupted to supply the necessary IGCs, it would imply a relatively high ICL surface brightness. What is more likely is that it is predominantly the halos of these galaxies that are stripped, and that the stellar halos have higher local S_N. A prediction of this scenario would be the presence of a large number of intermediate-luminosity galaxies in the cluster core that have relatively few GCs and compact GC systems. These galaxies might be detectable as outliers in the color–magnitude relation for early-type galaxies.

The color distribution of the IGCs also provides a clue. Although the IGCs are mostly blue, 20% of the IGCs are still red. This appears contrary to the simulations of Bekki & Yahagi (2006), which predicted a single metal-poor peak for the GCs with few metal-rich IGCs. The red IGCs we observe have a mean color consistent with the red GC populations found in the more massive early-type galaxies rather than in the dwarfs (Larsen et al. 2001; Peng et al. 2006). The fraction of red IGCs is also slightly higher than that in dwarfs. For Virgo early-type dwarfs with $M_V \gtrsim -18$, the mean fraction of red GCs is only 10%, and many have zero red GCs. Producing this many red IGCs solely from the disruption of low mass galaxies would be difficult. Stripping of GCs from the halos of more massive galaxies ($M_V \approx -19$) might be a more natural mechanism for producing the IGC population, although the stripping could not be too efficient, otherwise the ICL might be too red (c.f. the blue ICL color seen in Virgo by Rudick et al. 2010).

Mergers of these galaxies could also cause some metal-rich GCs to escape into intracluster space, although we are not able to differentiate between merging and stripping. Dissipational merging, with star formation, could also produce IGCs within gaseous tidal tails (e.g., Knapp et al. 2006), although for this mechanism to be important it would have to happen early in the formation of the cluster.

Although it is likely that dwarf galaxy disruption does play a role in supplying IGCs, the non-negligible fraction of red IGCs indicates that stripping and merging of intermediate-mass galaxies contributes a significant fraction of the population. Unfortunately, we do not currently have sufficient data to derive the full spatial profile of the IGC population itself, which would help determine the originating galaxy population, differentiate between merging, galaxy–galaxy interactions, and galaxy–cluster interactions, and also test whether the IGC radial density follows the overall mass density. More ACS imaging within the core and at larger radii would be extremely useful for this purpose.

7. CONCLUSIONS

We present the spatial distribution and color distribution of the globular cluster population in the Coma cluster core, from imaging obtained as part of the *HST*/ACS Coma Cluster Survey.

1. We discover a large population of GCs that do not appear to be associated with individual galaxies. After masking and statistically subtracting the GC systems of all member galaxies except the central galaxy, NGC 4874, we find that IGCs dominate the GC surface number density at galactocentric radii beyond $R > 130$ kpc. These IGCs appear to have a flat surface density profile out to the extent of our data ($R = 520$ kpc).
2. Using a Sérsic plus constant model fit to the radial profile, we estimate that there are 47,000 ± 1600 (random)

$^{+4000}_{-5000}$ (systematic) IGCs within 520 kpc and that these make up 70% of the central Coma cluster GC system (NGC 4874+IGCs). Including the GC systems of cluster members, we still estimate that IGCs make up 30%–45% of all GCs in the cluster core.

3. The color distribution of the IGCs is bimodal, with red GC fraction of 20%. The inner GCs around NGC 4874 also have a bimodal color distribution, although with a fairly red metal-poor population, and with equal numbers of blue and red GCs.
4. The reasonably high red fraction (20%) for the IGCs, and red colors of the metal-rich IGCs, suggests that the IGC population did not solely originate in dwarf galaxies, but at least some part was stripped from the halos of more massive galaxies.
5. These IGCs trace a large population of stars with an estimated surface brightness of $\mu_V \approx 27$ mag arcsec^{-2} (assuming $S_{N,\mathrm{IGC}} = 8$). The ICL makes up approximately half of the stellar luminosity and one-third of the stellar mass of the central system. The IGCs and ICL are associated with the build up of the central cluster galaxy and are likely the result of the continued growth and evolution of the cluster well after star formation has ceased.

We thank Naoyuki Tamura for sharing his surface density profile of the M87 GC system and Neal Miller for his helpful comments. We thank the referee for useful suggestions that improved the manuscript.

E.W.P. gratefully acknowledges support from the Peking University Hundred Talent Fund (985) and grant 10873001 from the National Natural Science Foundation of China, and thanks the Beijing Bookworm for their hospitality. T.H.P. acknowledges support from the National Research Council of Canada through the Plaskett Research Fellowship. D.C. is supported by STFC rolling grant PP/E001149/1 "Astrophysics Research at LJMU."

Support for program GO-10861 was provided through a grant from the Space Telescope Science Institute, which is operated by the Association for Research in Astronomy, Inc., under NASA contract NAS5-26555.

This research has made use of the NASA/IPAC Extragalactic Database (NED) which is operated by the Jet Propulsion Laboratory, California Institute of Technology, under contract with the National Aeronautics and Space Administration.

This publication makes use of data products from the Sloan Digital Sky Survey (SDSS). Funding for SDSS and SDSS-II has been provided by the Alfred P. Sloan Foundation, the Participating Institutions, the National Science Foundation, the U.S. Department of Energy, the National Aeronautics and Space Administration, the Japanese Monbukagakusho, the Max Planck Society, and the Higher Education Funding Council for England. The SDSS Web site is http://www.sdss.org/.

The SDSS is managed by the Astrophysical Research Consortium (ARC) for the Participating Institutions. The Participating Institutions are the American Museum of Natural History, Astrophysical Institute Potsdam, University of Basel, University of Cambridge, Case Western Reserve University, The University of Chicago, Drexel University, Fermilab, the Institute for Advanced Study, the Japan Participation Group, The Johns Hopkins University, the Joint Institute for Nuclear Astrophysics, the Kavli Institute for Particle Astrophysics and Cosmology, the Korean Scientist Group, the Chinese Academy of Sciences (LAMOST), Los Alamos National Laboratory, the Max-Planck-Institute for Astronomy (MPIA), the Max-Planck-Institute for Astrophysics (MPA), New Mexico State University, Ohio State University, University of Pittsburgh, University of Portsmouth, Princeton University, the United States Naval Observatory, and the University of Washington.

The Digitized Sky Surveys were produced at the Space Telescope Science Institute under U.S. Government grant NAG W-2166. The images of these surveys are based on photographic data obtained using the Oschin Schmidt Telescope on Palomar Mountain and the UK Schmidt Telescope. The plates were processed into the present compressed digital form with the permission of these institutions.

The National Geographic Society–Palomar Observatory Sky Atlas (POSS-I) was made by the California Institute of Technology with grants from the National Geographic Society.

The Second Palomar Observatory Sky Survey (POSS-II) was made by the California Institute of Technology with funds from the National Science Foundation, the National Geographic Society, the Sloan Foundation, the Samuel Oschin Foundation, and the Eastman Kodak Corporation.

The Oschin Schmidt Telescope is operated by the California Institute of Technology and Palomar Observatory.

Facility: *HST* (ACS)

APPENDIX

MASKING AND MODELING OF GLOBULAR CLUSTERS FROM COMA GALAXIES

A.1. Generating Masks

We first generate masks around bright galaxies in and around all of our fields. We define masked galaxies to be those with 200″ of an ACS field center and with $g_0 < 18$ ($M_g < -17$) as observed in the SDSS Data Release 6 (DR6) catalog. To be conservative, we choose all galaxies that meet these criteria, although nearly all at these bright magnitudes are cluster members. We are required to use a catalog external to our ACS survey because some large galaxies not observed by ACS, but just off the edge of a field, can contribute GCs to our observations.

For each galaxy, excluding the two giants NGC 4874 and 4889, we use as a crude measure of galaxy size the radius that encloses 50% of the Petrosian light ($R_{p,50}$). After experimenting with various mask sizes, we liberally mask an area corresponding to a circular aperture with a radius of $8R_{p,50}$. For a Sérsic profile with $n = 2$, this would mask 99% of the galaxy light. Even if the GC systems were twice the size of the galaxies, this would still mask ∼92% of the GC system. For three of the larger galaxies, the SDSS sizes are not reliable, so we manually adjusted the mask size. For NGC 4889, IC 4045, and 4908 we used mask radii of 230″, 68″, and 160″, respectively.

A.2. Simulated GC Spatial Distributions from Galaxies

For NGC 4889 in particular, the GC system is so large that a simple masking will not eliminate the contribution of its GCs. This is also the case for a few other bright galaxies. There is also the possibility that smaller but more numerous GC systems from the many dwarf galaxies in the cluster are contributing to the observed distribution of GCs. To account for this, we have simulated the composite GC distribution we would expect from the known galaxies in Coma.

We start with the Coma cluster galaxy catalog of Eisenhardt et al. (2007), who published $UBVRIzJHK_s$ photometry for Coma

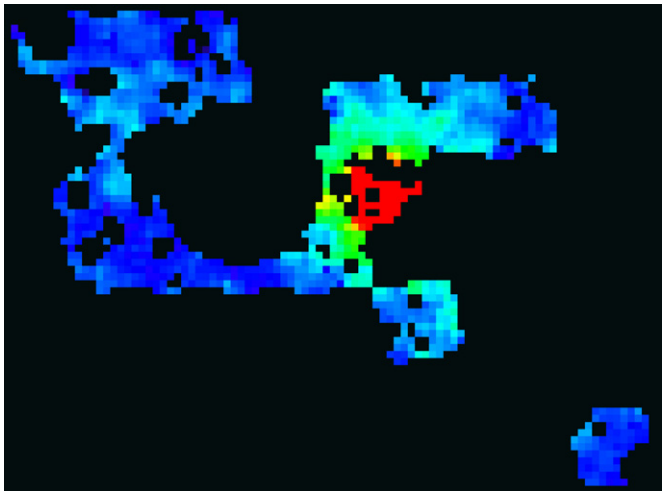

Figure 9. Smoothed spatial distribution of GCs in the Coma cluster core as in Figure 4 (30.′8 × 23.′0, 900 × 670 kpc), except with areas around bright galaxies masked, and modeled contribution from galactic GC systems subtracted. The area and surface densities in this image are used in the radial profile shown in Figure 5.

(A color version of this figure is available in the online journal.)

galaxies covering a region well matched to our cluster core mosaic. For this purpose, their catalog is superior to the SDSS data because Eisenhardt et al. (2007) specifically measured photometry of the Coma galaxies, many of which are too large for the SDSS pipeline to handle properly. Their catalog is complete to $M_V < -16$ mag and extends to $M_V < -14$ mag. We use their Tables 1 and 2 as the basis for our simulated GC systems. We assume that each galaxy in their catalog has a GC system that is circularly symmetric and has a radial number density distribution that follows a Sérsic (1968) profile with index $n = 2$, which is a good fit to the GC spatial density profiles of the Virgo giant ellipticals M87 and M49. The one exception to this is NGC 4889, for which it seems clear from Figure 3 that its associated GC systems are not spherical. For this galaxy, we assume that the spatial density distribution follows a Sérsic profile along the geometric mean radius, $\langle r \rangle = \sqrt{ab}$, where a and b are the major and minor axes, respectively. The ellipticity of NGC 4889 is $\epsilon = 0.379$ (Jorgensen et al. 1992), although we find that its GC systems are better described with higher ellipticity and use $\epsilon = 0.6$. For this galaxy, we do not need to model its GCs but can use the observed radial distribution of GCs from the WFPC2 observations of Harris et al. (2009).

We then estimate the GC specific frequency, S_N, for each galaxy based on its absolute V magnitude, M_V. We use a linear interpolation of the Virgo early-type galaxy S_N data presented in Table 3 of Peng et al. (2008), giving us an estimate of the total number of GCs in each galaxy. Although we do not make any adjustments for morphological type, most cluster members in the core are early types similar to the galaxies analyzed in Peng et al. (2008), and early types also generally have higher S_N than late-types.

Lastly, we determine an effective radius, R_e, for the GC system, also assuming that it scales with galaxy M_V. We used a second-order polynomial fit between R_e and M_V in which GC systems of more luminous galaxies are larger. We derived this relation using the GC systems of 100 Virgo cluster galaxies observed in the ACSVCS (Côté et al. 2004; Jordán et al. 2009). This survey observed early-type galaxies with a wide range of luminosities ($-22 < M_B < -15$). The spatial density profiles were fit with Sérsic profiles to derive the effective radius of the GC systems as a function of galaxy luminosity. The details of this relation and its derivation will appear in a subsequent paper (E. W. Peng et al. 2011, in preparation). The spatial extent of GC systems is generally larger than that of the stars and is consistent with previous measurements showing that the local S_N for giant ellipticals increases with galactocentric radius. With this estimate of R_e, we can then infer the contribution of GCs from galactic systems as a function of position in the central mosaic of observations.

Using the same spatial grid shown in Figure 4, we estimate the total number of GCs expected in each cell from *all* of the galaxies in the Eisenhardt et al. (2007) catalog (not including NGC 4874). We correct this number for the total observed area—accounting for unobserved and masked area—and the local GCLF completeness. For each cell, we thus have an estimate of the total number of observed GCs that could be contributed by the GC systems of known cluster galaxies.

We then use this simulated distribution of GCs to statistically subtract the contribution from "galactic" GCs. In each cell, we sample a Poisson distribution about the expected value, and then assign each GC a random position in the cell. Additionally, we mask regions around all the known galaxies, as described above, with the results shown in Figure 9. We do expect that some galactic GCs will contribute to the apparent intergalactic GC population, especially GCs from the other gE, NGC 4889, but the expected number and spatial distribution of the galactic GCs (i.e., concentrated around the galaxies) do not agree with the spatial uniformity and overall large numbers of GCs observed throughout the cluster core.

We also note that although our modeling of GC systems only extends to galaxies with $M_V < -14$ mag, this is unlikely to bias our final result. While it is true that S_N does tend to rise at lower luminosities, and some individual dEs have high S_N, the mean value is not very high. As shown by Miller & Lotz (2007) and Peng et al. (2008), dEs and dSphs have a very wide range of S_N, with some being high but many others quite ordinary or near zero. The mean S_N for dwarfs in the magnitude range that concerns us is ∼2. Studies of Local Group dwarfs show that at fainter than a certain luminosity ($M_B \approx -10$), dSphs do not appear to have GCs.

A.3. Systematic Errors from Modeling

The technique we use to account for the unmasked galactic GCs introduces a systematic uncertainty into our analysis. We can quantify this effect by varying the assumed parameters over a wide range of acceptable values. We detail this in this section, but our main point is that our conclusions are not particularly sensitive to the specific parameters assumed for the modeling of galactic GC systems, because if Coma early-type galaxies have the same range of specific frequencies as Virgo early-type galaxies, then there are simply not enough galactic GCs to account for all the GCs that we observe.

We have produced a range of plausible galactic GC populations, varying the Sérsic n index of the assumed profiles, the effective radius, R_e, and the specific frequencies of the galaxies, S_N. By varying the Sérsic index from $n = 1.0$ to $n = 4.0$ (exponential to de Vaucouleurs), the inferred number of IGCs varies from 47,000 to 44,000. The exponential profile is steepest in the outer regions and so gives the highest estimate for the IGC population. If we assume that all galactic GC systems have the shallower outer profiles of a de Vaucouleurs profile, then our inferred IGC population is smaller by ∼3000 GCs. This effect

is only at the peak-to-peak level of 6%–7% and is small enough to justify our choice of a single Sérsic index for our GCS models. A single $n = 2$ model gives us an inferred population of 46,500 IGCs, so we take the systematic error here to be $(^{+500}_{-3,000})$.

By varying the specific frequency, we affect the total number of galactic GCs. Our modeling uses the S_N–L relationship from Peng et al. (2008). Although there is no evidence that S_N for normal galaxies is different in the Coma cluster, we can make the assumption that S_N is systematically different from Virgo by ±20%. Doing so would change the number of IGCs by ±2000. This does not appreciably alter the significance of the detection. We include this in the systematic error budget.

We can also test the dependence of inferred IGC numbers on the effective radii of the GC systems. We can assume that the R_e of GC systems in Coma are a factor of two larger or smaller for a given galaxy luminosity than for their counterparts in Virgo (a fairly extreme assumption). If the GC systems are larger, the number of unmasked galactic GCs is increased and the number of IGCs will go down. Using this assumption in our modeling, the total number of IGCs changes by ±3000. Once again, the overall effect on the significance of our detection is rather small.

Given that our systematic errors are comparable to or larger than our Poisson errors (which are at the level of ±1600 GCs), it is important to include these in the error budget. Nevertheless, it is clear that the details of the modeling do not affect the conclusion that there is a significant detection of IGCs in the Coma core. By combining the estimated errors independently and in quadrature, we estimate that there is a combined systematic error of $^{+4000}_{-5000}$ IGCs. The inferred number of IGCs is thus 47,000 ± 1600 (random) $^{+4000}_{-5000}$ (systematic).

A.4. A Test of GC System Modeling

There are three outer ACS fields that we do not use for our background estimate because they are near larger Coma galaxies. Assuming that these fields have few or no IGCs, they present the opportunity to test the validity of our methodology. This test is not ideal, because NGC 4839 is a giant elliptical galaxy that is the dominant member of its subgroup, and our assumptions are most valid when we can average over many galaxies rather than be dominated by a luminous single galaxy. Nevertheless, we can apply the technique used to model the core region and check for consistency. Similar to NGC 4889, for which there are published measurements and no need to infer from scaling relations, we use the known S_N for NGC 4839 (Marín-Franch & Aparicio 2002), although for every other parameter and for all other galaxies in the region, we use our scaling relations. We take the same approach to modeling and masking as was done in the core, although since the Eisenhardt et al. (2007) catalog does not cover this region, we use an equivalent cut with SDSS. For each field, after subtracting the modeled GC population and the estimated background from the total counts, we should expect to have numbers statistically equivalent to zero. For these three fields, we obtain residual counts of 13 ± 9, 3 ± 11, and 10 ± 13, where the errors do not include the systematic errors as discussed above. We can assume that the systematic errors contribute roughly equally (or more) to the error budget. These numbers are satisfyingly consistent with zero, within the random and systematic errors. The predicted values do skew positive (with large errors), but this is likely a reflection of our systematic error, and is consistent with what we discuss in Appendix A.3. Over three fields, the residual is marginally significant over random errors, 26 ± 19 or when corrected for the full GCLF, 0.007 ± 0.005 kpc^{-2}. This is still 8× smaller than our measured IGC surface density, so any systematic residual at this level would not affect the significance of our measurement. Even if we were to adjust our model to increase the predicted number of GCs so as to match these fields, the impact on our result and the IGCs numbers would be small and within our quoted errors. Thus, we are reassured that our GC subtraction procedure and estimation of our uncertainties is robust.

REFERENCES

Adami, C., et al. 2005, A&A, 429, 39
Arnaboldi, M., Gerhard, O., Aguerri, J. A. L., Freeman, K. C., Napolitano, N. R., Okamura, S., & Yasuda, N. 2004, ApJ, 614, L33
Arnaboldi, M., Gerhard, O., Okamura, S., Kashikawa, N., Yasuda, N., & Freeman, K. C. 2007, PASJ, 59, 419
Ashman, K. M., Bird, C. M., & Zepf, S. E. 1994, AJ, 108, 2348
Balcells, M., et al. 2011, ApJ, submitted
Bassino, L. P., Cellone, S. A., Forte, J. C., & Dirsch, B. 2003, A&A, 399, 489
Bassino, L. P., Faifer, F. R., Forte, J. C., Dirsch, B., Richtler, T., Geisler, D., & Schuberth, Y. 2006, A&A, 451, 789
Beasley, M. A., Bridges, T., Peng, E., Harris, W. E., Harris, G. L. H., Forbes, D. A., & Mackie, G. 2008, MNRAS, 386, 1443
Bergond, G., et al. 2007, A&A, 464, L21
Bernstein, G. M., Nichol, R. C., Tyson, J. A., Ulmer, M. P., & Wittman, D. 1995, AJ, 110, 1507
Bekki, K., & Yahagi, H. 2006, MNRAS, 372, 1019
Bertin, E., & Arnouts, S. 1996, A&AS, 117, 393
Bildfell, C., Hoekstra, H., Babul, A., & Mahdavi, A. 2008, MNRAS, 389, 1637
Blakeslee, J. P. 1997, ApJ, 481, L59
Blakeslee, J. P. 1999, AJ, 118, 1506
Blakeslee, J. P., & Tonry, J. T. 1995, ApJ, 442, 579
Blakeslee, J. P., Tonry, J. L., & Metzger, M. R. 1997, AJ, 114, 482
Calcáneo-Roldán, C., Moore, B., Bland-Hawthorn, J., Malin, D., & Sadler, E. M. 2000, MNRAS, 314, 324
Carter, D., et al. 2008, ApJS, 176, 424
Castro-Rodriguéz, N., Arnaboldi, M., Aguerri, J. A. L., Gerhard, O., Okamura, S., Yasuda, N., & Freeman, K. C. 2009, A&A, 507, 621
Chiboucas, K., et al. 2010, in Proc. Conf. on A Universe of Dwarf Galaxies, Lyon, France, 14–18 June 2010 (arXiv:1009.3950)
Collins, C. A., et al. 2009, Nature, 458, 603
Côté, P., et al. 2004, ApJS, 153, 223
Da Rocha, C., & Mendes de Oliveira, C. 2005, MNRAS, 364, 1069
De Lucia, G., & Blaizot, J. 2007, MNRAS, 375, 2
de Vaucouleurs, G., & de Vaucouleurs, A. 1970, Astrophys. Lett., 5, 219
Demarco, R., Magnard, F., Durret, F., & Márquez, I. 2003, A&A, 407, 437
Doherty, M., et al. 2009, A&A, 502, 771
Drinkwater, M. J., Gregg, M. D., Hilker, M., Bekki, K., Couch, W. J., Ferguson, H. C., Jones, J. B., & Phillipps, S. 2003, Nature, 423, 519
Durrell, P. R., Ciardullo, R., Feldmeier, J. J., Jacoby, G. H., & Sigurdsson, S. 2002, ApJ, 570, 119
Eisenhardt, P. R., De Propris, R., Gonzalez, A. H., Stanford, S. A., Wang, M., & Dickinson, M. 2007, ApJS, 169, 225
Feldmeier, J. J., Ciardullo, R., & Jacoby, G. H. 1998, ApJ, 503, 109
Feldmeier, J. J., Ciardullo, R., Jacoby, G. H., & Durrell, P. R. 2004a, ApJ, 615, 196
Feldmeier, J. J., Mihos, J. C., Morrison, H. L., Harding, P., Kaib, N., & Dubinski, J. 2004b, ApJ, 609, 617
Feldmeier, J. J., Mihos, J. C., Morrison, H. L., Rodney, S. A., & Harding, P. 2002, ApJ, 575, 779
Ferguson, H. C., Tanvir, N. R., & von Hippel, T. 1998, Nature, 391, 461
Fruchter, A. S., & Hook, R. N. 2002, PASP, 114, 144
Fukugita, M., Shimasaku, K., & Ichikawa, T. 1995, PASP, 107, 945
Gallagher, J. S., III, & Ostriker, J. P. 1972, AJ, 77, 288
Gal-Yam, A., Maoz, D., Guhathakurta, P., & Filippenko, A. V. 2003, AJ, 125, 1087
Gebhardt, K., & Kissler-Patig, M. 1999, AJ, 118, 1526
Georgiev, I. Y., Goudfrooij, P., Puzia, T. H., & Hilker, M. 2008, AJ, 135, 1858
Georgiev, I. Y., Puzia, T. H., Hilker, M., & Goudfrooij, P. 2009, MNRAS, 392, 879
Gerhard, O., Arnaboldi, M., Freeman, K. C., Okamura, S., Kashikawa, N., & Yasuda, N. 2007, A&A, 468, 815
Gnedin, O. Y. 2003, ApJ, 582, 141
Gonzalez, A. H., Zabludoff, A. I., & Zaritsky, D. 2005, ApJ, 618, 195
Gonzalez, A. H., Zaritsky, D., & Zabludoff, A. I. 2007, ApJ, 666, 147

Gregg, M. D., & West, M. J. 1998, Nature, 396, 549
Gregg, M. D., et al. 2009, AJ, 137, 498
Hammer, D., et al. 2010, ApJS, 191, 143
Harris, W. E. 1991, ARA&A, 29, 543
Harris, W. E. 2009, ApJ, 703, 939
Harris, W. E., Kavelaars, J. J., Hanes, D. A., Hesser, J. E., & Pritchet, C. J. 2000, ApJ, 533, 137
Harris, W. E., Kavelaars, J. J., Hanes, D. A., Pritchet, C. J., & Baum, W. A. 2009, AJ, 137, 3314
Harris, W. E., & van den Bergh, S. 1981, AJ, 86, 1627
Haşegan, M., et al. 2005, ApJ, 627, 203
Hilker, M., Baumgardt, H., Infante, L., Drinkwater, M., Evstigneeva, E., & Gregg, M. 2007, A&A, 463, 119
Jedrzejewski, R. I. 1987, MNRAS, 226, 747
Jordán, A., West, M. J., Côté, P., & Marzke, R. O. 2003, AJ, 125, 1642
Jordán, A., et al. 2004, ApJS, 154, 509
Jordán, A., et al. 2006, ApJ, 651, L25
Jordán, A., et al. 2007, ApJS, 171, 101
Jordán, A., et al. 2009, ApJS, 180, 54
Jorgensen, I., Franx, M., & Kjaergaard, P. 1992, A&AS, 95, 489
Kavelaars, J. J., Harris, W. E., Hanes, D. A., Hesser, J. E., & Pritchet, C. J. 2000, ApJ, 533, 125
Knapp, G. R., et al. 2006, AJ, 131, 859
Koekemoer, A. M., Fruchter, A. S., Hook, R. N., & Hack, W. 2002, in The 2002 *HST* Calibration Workshop: Hubble after the Installation of the ACS and the NICMOS Cooling System, Space Telescope Science Institute, Baltimore, Maryland, 2002 October 17 and 18, ed. S. Arribas, A. Koekemoer, & B. Whitmore (Baltimore, MD: Space Telescope Science Institute), 339
Kormendy, J., & Bahcall, J. N. 1974, AJ, 79, 671
Krick, J. E., & Bernstein, R. A. 2007, AJ, 134, 466
Larsen, S. S., Brodie, J. P., Huchra, J. P., Forbes, D. A., & Grillmair, C. J. 2001, AJ, 121, 2974
Lee, M. G., Park, H. S., & Hwang, H. S. 2010, Science, 328, 334
Lin, Y.-T., & Mohr, J. J. 2004, ApJ, 617, 879
Liu, C., Peng, E. W., Jordán, A., Ferrarese, L., Blakeslee, J. P., Côté, P., & Mei, S. 2011, ApJ, in press (arXiv:1012.2634)
Lopez-Cruz, O., Yee, H. K. C., Brown, J. P., Jones, C., & Forman, W. 1997, ApJ, 475, L97
Madrid, J. P., et al. 2010, ApJ, 722, 1707
Marín-Franch, A., & Aparicio, A. 2002, ApJ, 568, 174
Marín-Franch, A., & Aparicio, A. 2003, ApJ, 585, 714
Matthews, T. A., Morgan, W. W., & Schmidt, M. 1964, ApJ, 140, 35
Mattila, K. 1977, A&A, 60, 425
McLachlan, G. J., & Basford, K. E. 1988, Mixture Models: Inference and Application to Clustering (New York: Dekker)
McLaughlin, D. E. 1999, AJ, 117, 2398
Melnick, J., Hoessel, J., & White, S. D. M. 1977, MNRAS, 180, 207
Mendez, R. H., Guerrero, M. A., Freeman, K. C., Arnaboldi, M., Kudritzki, R. P., Hopp, U., Capaccioli, M., & Ford, H. 1997, ApJ, 491, L23
Merritt, D. 1984, ApJ, 276, 26
Merritt, D., Graham, A. W., Moore, B., Diemand, J., & Terzić, B. 2006, AJ, 132, 2685
Mieske, S., et al. 2008, A&A, 487, 921
Mihos, J. C., Harding, P., Feldmeier, J., & Morrison, H. 2005, ApJ, 631, L41
Mihos, J. C., Janowiecki, S., Feldmeier, J. J., Harding, P., & Morrison, H. 2009, ApJ, 698, 1879
Miller, B. W., & Lotz, J. M. 2007, ApJ, 670, 1074
Monaco, P., Murante, G., Borgani, S., & Fontanot, F. 2006, ApJ, 652, L89
Moore, B., Diemand, J., Madau, P., Zemp, M., & Stadel, J. 2006, MNRAS, 368, 563
Moore, B., Lake, G., & Katz, N. 1998, ApJ, 495, 139
Murante, G., Giovalli, M., Gerhard, O., Arnaboldi, M., Borgani, S., & Dolag, K. 2007, MNRAS, 377, 2
Neill, J. D., Shara, M. M., & Oegerle, W. R. 2005, ApJ, 618, 692
Oemler, A., Jr. 1976, ApJ, 209, 693
Okamura, S., et al. 2002, PASJ, 54, 883
Peng, E. W., Ford, H. C., & Freeman, K. C. 2004, ApJ, 602, 705
Peng, E. W., et al. 2006, ApJ, 639, 95
Peng, E. W., et al. 2008, ApJ, 681, 197
Peng, E. W., et al. 2009, ApJ, 703, 42
Price, J., et al. 2009, MNRAS, 397, 1816
Puchwein, E., Springel, V., Sijacki, D., & Dolag, K. 2010, MNRAS, 406, 936
Purcell, C. W., Bullock, J. S., & Zentner, A. R. 2007, ApJ, 666, 20
Puzia, T. H., Kissler-Patig, M., Thomas, D., Maraston, C., Saglia, R. P., Bender, R., Goudfrooij, P., & Hempel, M. 2005, A&A, 439, 997
Puzia, T. H., & Sharina, M. E. 2008, ApJ, 674, 909
Rhode, K. L., & Zepf, S. E. 2001, AJ, 121, 210
Rhode, K. L., Zepf, S. E., Kundu, A., & Larner, A. N. 2007, AJ, 134, 1403
Rudick, C. S., Mihos, J. C., Frey, L. H., & McBride, C. K. 2009, ApJ, 699, 1518
Rudick, C. S., Mihos, J. C., Harding, P., Feldmeier, J. J., Janowiecki, S., & Morrison, H. L. 2010, ApJ, 720, 569
Rudick, C. S., Mihos, J. C., & McBride, C. 2006, ApJ, 648, 936
Schlegel, D. J., Finkbeiner, D. P., & Davis, M. 1998, ApJ, 500, 525
Schuberth, Y., Richtler, T., Bassino, L., & Hilker, M. 2008, A&A, 477, L9
Scoville, N., et al. 2007, ApJS, 172, 38
Seigar, M. S., Graham, A. W., & Jerjen, H. 2007, MNRAS, 378, 1575
Sérsic, J. L. 1968, Atlas de Galaxias Australes (Cordoba: Observatorio Astronomico)
Seth, A., Olsen, K., Miller, B., Lotz, J., & Telford, R. 2004, AJ, 127, 798
Sharina, M. E., Puzia, T. H., & Makarov, D. I. 2005, A&A, 442, 85
Sirianni, M., et al. 2005, PASP, 117, 1049
Smith, R. J., et al. 2008, MNRAS, 386, L96
Sommer-Larsen, J., Romeo, A. D., & Portinari, L. 2005, MNRAS, 357, 478
Spitler, L. R., & Forbes, D. A. 2009, MNRAS, 392, L1
Stanghellini, L., González-García, A. C., & Manchado, A. 2006, ApJ, 644, 843
Stetson, P. B. 1987, PASP, 99, 191
Tamura, N., Sharples, R. M., Arimoto, N., Onodera, M., Ohta, K., & Yamada, Y. 2006, MNRAS, 373, 601
Theuns, T., & Warren, S. J. 1997, MNRAS, 284, L11
Thuan, T. X., & Gunn, J. E. 1976, PASP, 88, 543
Thuan, T. X., & Kormendy, J. 1977, PASP, 89, 466
Trentham, N., & Mobasher, B. 1998, MNRAS, 293, 53
Uson, J. M., Boughn, S. P., & Kuhn, J. R. 1991, ApJ, 369, 46
Vilchez-Gomez, R., Pello, R., & Sanahuja, B. 1994, A&A, 283, 37
Welch, G. A., & Sastry, G. N. 1972, ApJ, 171, L81
West, M. J. 1993, MNRAS, 265, 755
West, M. J., Cote, P., Jones, C., Forman, W., & Marzke, R. O. 1995, ApJ, 453, L77
West, M. J., et al. 2011, ApJ, submitted
Whiley, I. M., et al. 2008, MNRAS, 387, 1253
Williams, B. F., et al. 2007, ApJ, 654, 835
Willman, B., Governato, F., Wadsley, J., & Quinn, T. 2004, MNRAS, 355, 159
Woodley, K. A., Harris, W. E., Puzia, T. H., Gómez, M., Harris, G. L. H., & Geisler, D. 2010, ApJ, 708, 1335
Yahagi, H., & Bekki, K. 2005, MNRAS, 364, L86
Yang, X., Mo, H. J., & van den Bosch, F. C. 2009, ApJ, 693, 830
Zibetti, S., White, S. D. M., Schneider, D. P., & Brinkmann, J. 2005, MNRAS, 358, 949
Zwicky, F. 1951, PASP, 63, 61